Energy & Environmental Science

ROYAL SOCIETY OF CHEMISTRY

REVIEW

View Article Online
View Journal | View Issue

Cite this: *Energy Environ. Sci.*, 2021, **14**, 5191

Review and outlook on high-entropy alloys for hydrogen storage

Felipe Marques, [a] Mateusz Balcerzak, [ab] Frederik Winkelmann, [a] Guilherme Zepon [cd] and Michael Felderhoff *[a]

Recently, a new class of alloys, namely, high-entropy alloys (HEAs), started to be investigated for hydrogen storage as they can form metal hydrides. Considering that the properties of metal hydrides are greatly influenced by the type of phase formed, and chemical composition, HEAs (with their vastness of compositions) present a high potential for developing promising materials for this application. A crucial aspect in assessing the potential of these alloys is the effective compositional design and synthesis. Here, we evaluate the methods used for obtaining HEAs for hydrogen storage and, based on the most advanced discussions of phase formation and stability in HEAs, we expose some strategies for a better assessment of the vast compositional field. Moreover, we present and discuss the first attempts to model the hydrogenation properties of HEAs using thermodynamics and data science. The development of these kinds of predictive tools is paramount for exploring HEAs' potential for hydrogen storage. To date, the most promising HEA compositions can be classified into three classes: body-centered cubic HEAs, lightweight HEAs, and intermetallic HEAs.

Received 21st May 2021,
Accepted 31st August 2021

DOI: 10.1039/d1ee01543e

rsc.li/ees

Broader context

Hydrogen storage is a key issue in the context of the hydrogen economy. In this context, metal hydrides are considered a long-term alternative for solid-state hydrogen storage, as they can store hydrogen reversibly and safely with high volumetric densities. However, to date, most of the metal hydrides studied are not suitable for hydrogen storage for either presenting limited storage capacity (gravimetric) or properties that require non-acceptable physical conditions to store hydrogen reversibly. Different strategies have been investigated for tailoring the properties of metal hydrides, and one of the most effective is chemical composition modification (alloying, for instance). In this context, a new class of alloys, namely, high-entropy alloys (HEAs), has been investigated for hydrogen storage. It may provide a promising way further to investigate solid-state hydrogen storage. One of the main aspects of HEAs is the vastness of compositional configurations that form simple crystalline structures. It provides great possibilities to adjust the properties of the hydrides. However, for efficient exploration of this alloy concept for hydrogen storage, alloy design based on predictive tools is fundamental, as it is presented in this review on HEAs for hydrogen storage.

Introduction

Main definitions and general overview

A hydrogen and fuel cell-based economy holds a promising prospect for a more environmentally friendly energy sector, still dependent on fossil fuels. The safe, effective, and economically viable transition to the hydrogen-based economy is highly dependent on hydrogen storage. Among the options for hydrogen storage, the solid-state-based method is one of the most promising as, besides other aspects, more hydrogen per volume unit can be stored than in the liquid or gas states.[1] Since this approach has been introduced, a wide variety of metal hydrides have been investigated as solid-state hydrogen storage materials.[1,2] Most of the research on these materials has been focused on investigating and developing metal hydrides with improved gravimetric and volumetric capacities, reasonable thermodynamics and kinetics of hydrogen absorption/desorption, and long-term cycling stability.[2–5] Among the most promising alloy-based metal hydrides, Mg-based materials have the advantage of high gravimetric capacities, but their unfavorable thermodynamic properties (high temperatures are required to store hydrogen reversibly) prevent their broad application.[5] Solid solution alloys (especially the V-based ones) also present promising hydrogen storage properties. However,

[a] *Max-Planck-Institut für Kohlenforschung, Kaiser-Wilhelm-Platz 1, 45470 Mülheim an der Ruhr, Germany. E-mail: felderhoff@mpi-muelheim.mpg.de*
[b] *Institute of Materials Science and Engineering, Poznan University of Technology, Jana Pawla II No. 24, 61-138 Poznan, Poland*
[c] *Department of Materials Engineering, Federal University of São Carlos, Rod. Washington Luis, km 235, CEP: 13565-905, São Carlos, SP, Brazil*
[d] *Graduate Program of Materials Science and Engineering, Federal University of São Carlos, Rod. Washington Luis, km 235, CEP: 13565-905, São Carlos, SP, Brazil*

the hydrides formed are too stable under ambient conditions.[6] Intermetallic compounds (such as TiFe and $LaNi_5$) present good hydrogen storage reversibility under near ambient conditions, but they suffer from low gravimetric capacities (due to the presence of heavy elements as in $LaNi_5$ or unfavorable thermodynamics as for TiFe).[7,8] For a comprehensive review of the recent development on metal hydrides, the reader is also encouraged to check the following ref. 9. Recently, a new class of alloys, namely, high-entropy alloys (HEAs), started to be investigated for their hydrogen storage properties.[10–37] Following the first report in 2010, only a few papers focusing on HEAs were published in the next five years. However, the interest in this research field has recently increased (since 2016), resulting in a growing number of articles published each year (see Fig. 1).

In HEAs, multiple elements are used in the compositions, and these elements are usually present in equiatomic or near equiatomic fractions. This idea of alloying with multi-principal elements was proposed simultaneously by Cantor *et al.*[38] and Yeh *et al.*,[39] although the high-entropy hypothesis was first suggested by Yeh's group. The proposed hypothesis was that by mixing multiple elements in near equiatomic proportion, the configurational entropy would be increased to the level sufficient to overcome the enthalpies of compound formation (intermetallics).[39] According to this, the formation of concentrated disordered solid solutions would be favored, and the presence of secondary intermetallic phases limited. The preference for solid solutions over intermetallics, in the original proposal, is based on the mechanical properties of these structures (intermetallics are usually brittle).[39] Based on that, HEAs were defined as alloys that contain five or more elements in atomic fraction between 5 and 35 at%.[39] While testing the high-entropy alloy hypothesis, it turned out that besides configurational entropy other entropic contributions (vibrational, magnetic, and electronic) and mixing enthalpies

Felipe Marques

Felipe Marques received his MS degree in Materials Science and Engineering from the Federal University of São Carlos (UFSCar), Brazil in 2020. He is currently a PhD student in the Department of Heterogeneous Catalysis at Max-Planck-Institut für Kohlenforschung, Germany. His current research activities are focused on the design, synthesis, and characterization of high-entropy alloys for hydrogen storage and unstable metal hydrides for hybrid hydrogen storage systems.

Mateusz Balcerzak

Mateusz Balcerzak received his PhD degree from Poznan University of Technology (PUT), Poland in 2016. Later on, he worked as a Postdoctoral researcher at PUT and Catalan Institute of Nanoscience and Nanotechnology, Spain. In 2020 he joined Max-Planck-Institut für Kohlenforschung, Germany as a Postdoctoral researcher. His research focuses on amorphous and nanocrystalline materials synthesized by mechanochemical synthesis – mostly according to their utility as hydrogen storage systems and Ni–MH secondary batteries. Mateusz Balcerzak currently works on high-entropy alloys for hydrogen storage and metal hydrides for hydrogen separation from gas mixtures.

Frederik Winkelmann

Frederik Winkelmann received his MS degree in Nanoengineering from the University of Duisburg-Essen in 2017. He is currently a PhD student in the Department of Heterogeneous Catalysis at Max-Planck-Institut für Kohlenforschung and is part of the International Max Planck Research School for Interface Controlled Materials for Energy Conversion (IMPRS-SurMat). His current research activities include the synthesis and characterization of high-entropy alloys with respect to their hydrogen storage properties.

Guilherme Zepon

Guilherme Zepon is an Assistant Professor at the Department of Materials Engineering of the Federal University of São Carlos (DEMa-UFSCar) in Brazil since 2016. In 2018, he was awarded a grant by the Serrapilheira Institute to develop the research project entitled "Design of high entropy alloys for hydrogen storage applications". His research focuses on the development of new and optimized metallic alloys through computational and experimental methods.

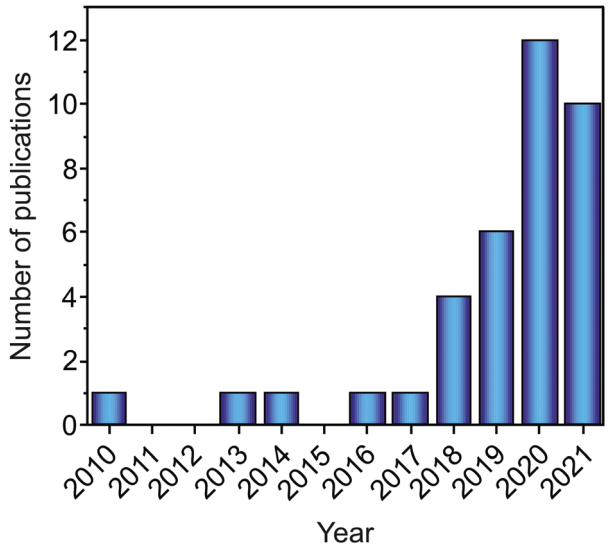

Fig. 1 Number of articles published per year in 2010–2021 (until April) with "high-entropy alloy" or "multi-principal element alloy" or "complex concentrated alloy" and "hydrogen storage" in the title, keywords, and abstract. Source: Scopus.

could play an essential role in the phase formation and stability of HEAs.[40]

Alternative names have been proposed to HEAs, such as multi-principal element alloys (MPEAs) and complex concentrated alloys (CCAs). Moreover, recently the term medium-entropy alloys (MEAs) has been proposed for the alloys that present four or fewer elements in equiatomic or near equiatomic fractions.[41,42] In the present work, to acknowledge the contributions of those who first proposed this alloy concept, we decided to use the name HEAs for the materials we focused on in our discussions. This nomenclature is used even in the case of intermetallic forming compositions to reference the use of the multiple main elements concept, although one has to consider that due to ordering in the structure of intermetallics, high entropy is unlikely.[40] We also suggested a standard way for reporting HEA compositions for hydrogen storage. According to this, the elements in the compositions appear in increasing order of atomic number. These suggestions were included in the tables of this review (in the text, the compositions are shown as they were reported in the original papers). The first column (from left to right) of the tables presents the normalized compositions following the suggestion we propose, and in the column next to it, the nominal compositions are shown as they were reported in the original papers.

To date, most HEAs have been investigated regarding their mechanical properties for structural applications. However, the interest in their functional properties has been increasing recently. HEAs are currently studied as diffusion barriers, catalysts, hydrogen storage materials, among others.[40]

The rationale for investigating hydrogen storage properties of HEAs

The concept of tuning the properties of materials *via* alloying is not new. In the research and development of materials for solid-state hydrogen storage, it has been evident that materials properties can be largely modified by adding new elements.[4] A great effort has been put into investigations of binary and ternary systems based on Mg, alanates, amides, imides and borohydrides, and intermetallic systems, such as $LaNi_5$, TiFe, and Ti- and Zr-based ones.[2] To some extent, multi-component alloy systems have also been explored.[43–45] As understood here, multicomponent alloy systems are those based on three or more elements in which there is a base element or base elements, and the remaining are present just in small fractions. This definition is not meant to be exhaustive but just to place the alloys in the context of the discussions performed in this work. In these multicomponent alloys, the elements are usually alloyed together to form solid solutions or multicomponent intermetallics with enhanced hydrogen storage properties.[46–48] In recent decades, the knowledge of tuning metal hydride properties has expanded significantly, and important developments have been achieved by investigating multicomponent systems.[2,46] However, the multicomponent approach has been mostly limited to exploring the effect of minor alloying additions on the hydrogen storage properties of well-known metal hydride systems. Moreover, this process has been highly dependent on costly and time-consuming systematic investigations.[2,46,49,50]

The HEA approach highlighted the vast number of unexplored compositions located in the central regions of multicomponent phase diagrams (multicomponent here refers to the multiple elements in these diagrams). It also stimulated the discussion of the fundamentals and tools for assessing this vast domain of uncharted compositions that can form simple crystalline structures.[51] In terms of materials for hydrogen storage, these aspects (vast compositional domain with the formation of simple crystalline structures) have indicated new possibilities for adjusting the properties of the materials. Improved hydrogen storage properties in HEAs, such as increased gravimetric capacity at moderate conditions and complete reversibility at room temperature without activation processes, have already been reported.[29,35]

Michael Felderhoff

Michael Felderhoff studied chemistry at the University of Essen, Germany, where he completed his doctorate in 1993 in organic chemistry. After two additional years in Essen, he carried out postdoctoral studies at the Universities of Tübingen and Osnabrück. Since 1999, he has been a member of the hydrogen storage group at the Max-Planck-Institut für Kohlenforschung. His research interests include mechanochemistry and the development of new metal hydride systems for hydrogen and heat storage.

In addition, the new HEA investigations have been shedding light on the average and local interactions between the hosting multi-principal elements and hydrogen and on how these interactions affect the storage properties of the alloy.[30,32,33] Thus, one could envision that specific HEA composition could be designed based on their predicted properties for particular hydrogen storage applications in the future. Given the rapid insertion of computational and machine learning tools into scientific investigations,[52] which also covers the hydrogen storage field,[53] the HEA concept, with its vast possibilities, could be significantly explored effectively with the aid of these powerful tools.

For instance, the remaining scientific and technological challenges related to hydrogen storage for future mobility require the development of new materials and storage concepts, as discussed in detail in these two ref. 54 and 55. In this context, investigations focused on HEA compositions that could present increased gravimetric capacity (around 4 wt% H_2), and high equilibrium pressures (allowing the use with 35 MPa pressurized tanks) would be highly beneficial for the development of this hydrogen storage field.[56]

Alloy design, synthesis, and promising HEA classes

Although most of the HEAs investigated so far (in the broad HEA field) were multi-phase alloys, much effort has been put into understanding how single-phase forming compositions can be designed so that fundamental mechanisms and properties could be elucidated without the confounding effects of secondary phases.[40,51] It has also been the case with the investigations of HEAs for hydrogen storage since besides the simplification aspect (of studying one phase rather than multiple ones), there has been little evidence that interaction of multiple phases enhances the hydrogen properties of such alloys greatly, although it cannot be ruled out.

Among the methods developed for the design of single-phase HEAs, the most reported in the studies for hydrogen storage are the empirical method (which relates the phase formation with a set of parameters: atomic size mismatch (δ), valence electron concentration (VEC), Pauling electronegativities (χ_p), and mixing enthalpies),[11,12,15,17,22,24] and the CALPHAD method (which is a software-based technique for calculation of phase diagrams based on thermodynamic models).[29,34] Besides this, recently, two methods for predicting the hydrogenation properties of HEAs have been developed, and they may improve the compositional design.[57,58] One employs a model based on thermodynamics and atomistic to predict the thermodynamic properties of hydrogenation/dehydrogenation of HEAs and their storage capacity. The other aims to predict the same properties of HEAs based on a data-driven approach that employs machine learning techniques. After the design, most of the compositions have been synthesized by arc melting, although high energy processes, such as high energy ball milling (HEBM) and high-pressure torsion (HPT), besides laser engineered net shaping (LENS), have also been employed.

In this paper, we classified the HEAs for hydrogen storage into three groups: body-centered cubic (BCC) HEAs, lightweight HEAs, and intermetallic HEAs, as can be seen in Fig. 2 (structure drawn using VESTA[59]). These groups are connected to the traditional metal hydride forming alloys and, to some extent, are influenced by the knowledge built so far (most of the promising traditional metal hydrides are based on BCCs, intermetallics, or lightweight alloys).[2,3,19] BCC HEAs and intermetallic HEAs are named according to the crystal structure that they form (BCC solid solutions and ordered intermetallic structures, respectively). The third one, lightweight HEAs, is not related to a specific crystal structure but to the presence of light elements incorporated into HEA's structure. Research on lightweight HEAs focuses mainly on improving the hydrogen storage gravimetric capacity *via* reducing the molar weight of the alloys. Since lightweight HEAs is not correlated to any specific crystal structure, it can contain HEAs with BCC, FCC and intermetallic structures. Nevertheless, up to date, most of the lightweight HEAs reported crystalizes in BCC structure. It is important to note that due to the particular scope of research on lightweight HEAs these studies were separated from the 'BCC HEAs' section.

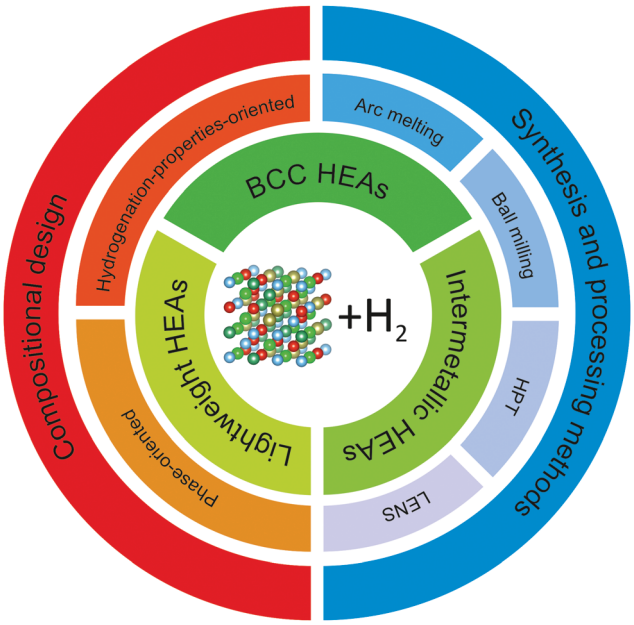

Fig. 2 Scheme indicating the concepts of compositional design, synthesis and processing methods, and HEA classes.[59]

In the following sections of this paper, the compositional design of HEAs and their synthesis methods are discussed. Within the compositional design, we present and discuss the attempts to predict the hydrogen storage properties of HEAs with the aid of thermodynamic modeling and data-driven modeling, showing how these methods may help to boost the development of promising materials for hydrogen storage.

Furthermore, each class of HEAs is critically discussed concerning phase formation and stability of the alloy and hydride, storage capacity, activation, kinetics, and cyclability. As an example of how each of these aspects is investigated in hydrogen storage materials, refer to this ref. 7. Along with the

discussions, perspectives are given to contribute to the development of this promising research field.

Methods for compositional design and synthesis processes

Some new HEA systems have already been deeply investigated regarding their hydrogen storage properties.[13,22,24,35] However, the recent investigations have not even scratched the surface of the possible compositional combinations that the HEA approach provides.

In the research and development of alloys for hydrogen storage, the interaction of the individual elements with hydrogen (represented mainly by the enthalpy of hydride formation) has guided the selection of the set of elements to be considered for compositional design.[4] The elements can be divided between hydride (A) and non-hydride forming (B) elements, as illustrated in Fig. 3. For the classification of A- and B-type elements, the respective enthalpies of formation for binary hydrides are considered, which take into account the tendency of forming a hydride. According to this concept, the A-type elements have lower values of enthalpy of formation and a higher tendency to form a hydride phase. In contrast, the B-type elements have higher values of enthalpy of formation, which makes hydride phase formation more difficult. The affinity of the alloy with hydrogen (given by the enthalpy of hydride formation) can be tuned *via* mixing elements with different enthalpies of hydride formation.[4,53] This knowledge accompanied the discovery of new HEA compositions for hydrogen storage.[15,28] In specific cases, as in the lightweight HEAs, other properties, such as the molar weight of the elements, also play an important role in the selection of the elements for the alloy design.[15,28,30,35,36] These approaches are in line with the well-established practice to investigate different metal hydride systems.[2,4] However, one particular aspect of HEAs is that the synthesis of single-phase alloys from the mixture of multi-principal elements has been considered highly desirable.[10,15,28–30,34]

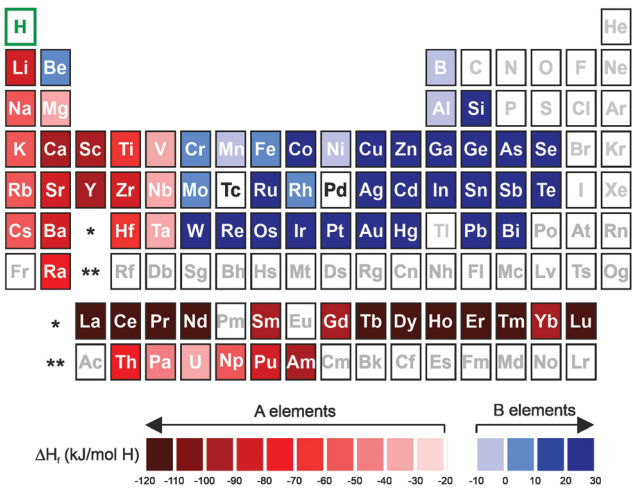

Fig. 3 Periodic table with relative subdivision of the A- and B-type elements, taking into account the grouping according to the enthalpies of formation of the binary metal hydrides.[4,7,117] A-type elements represented in shades of red, and B-type elements in shades of blue.

Given this context, so far, the design of HEAs for hydrogen storage has been, to some extent, still dependent on chemical intuition and costly and time-consuming try-and-error experimentation approaches.[57] However, as shown in the following sections, promising tools for improving the design of these alloys have been developed. Considering this, it is utterly necessary to assess and possibly improve these compositional design methods for efficient exploration of the uncharted central regions of multicomponent phase diagrams.

Furthermore, the formation of favorable microstructures for the intended application is directly related to the applied synthesis and processing methods.[22,53] Consequently, the impact of these processes on the obtained phases and microstructures in HEAs should be investigated, and whenever possible, their correlation with the compositional design method should be evaluated.

Phase-oriented compositional design

In the broad HEA field (considering all kinds of applications), the design of single-phase materials is preferable based on the assumption that secondary phases (mostly intermetallic compounds) would be detrimental to their properties. Therefore, a few methods for obtaining single-phase alloys have been suggested, and they can be divided into empirical, thermodynamic, and atomistic models, discussed in detail elsewhere.[40] As already mentioned, in the hydrogen storage field, the preference for single-phase is based on the simplification aspect of this approach (no confounding behavior of different phases). Moreover, there is little evidence that multi-phases are highly advantageous in developing alloys for hydrogen storage.[28,46] Certain crystalline phases, such as BCC, C14 and C15 Laves, and hexagonal close-packed (HCP), are favored in the alloy design since they are known as suitable for hydrogen storage.[2]

So far, the most cited method associated with the investigation of new HEAs for hydrogen storage is the empirical one.[10,11,14,15,21,30] The empirical approach is fundamentally influenced by the Hume-Rothery rules for obtaining solid solution alloys.[40] According to these rules, the formation of extended solid solutions is favored when alloys contain elements with similar atomic sizes, electronegativities, and valences, along with the same crystalline structures.[40,60] Likewise, in the empirical approach, terms for the differences in δ, electronegativity (δ_χ) and VEC, as well as some thermodynamic parameters, are calculated based on the alloy composition.[40,61–63] Among the thermodynamic parameters, the enthalpy of mixing (ΔH_{mix}) and an Ω parameter that correlates the enthalpy of mixing, the entropy of mixing (ΔS_{mix}) and melting temperature (T_m), are usually calculated.[40,64] All these parameters can be determined using the following

equations

$$\delta = \sqrt{\sum c_i \left(1 - \frac{r_i}{\bar{r}}\right)^2} \times 100 \quad (1)$$

$$\delta_\chi = \sqrt{\sum c_i \left(1 - \frac{\chi_i}{\bar{\chi}}\right)^2} \times 100 \quad (2)$$

$$\mathrm{VEC} = \sum c_i \mathrm{VEC}_i \quad (3)$$

$$\Delta H_{\mathrm{mix}} = \sum_{i<j} 4 H_{ij} c_i c_j \quad (4)$$

$$\Omega = \frac{T_{\mathrm{m}} \Delta S_{\mathrm{mix}}}{|\Delta H_{\mathrm{mix}}|} \quad (5)$$

where $T_{\mathrm{m}} = \sum_{i-1}^{n} c_{i(T_{\mathrm{m}})_i}$ and $\Delta S_{\mathrm{mix}} = -R \sum c_i \ln c_i$

In the formulas, r_i, χ_i and VEC_i stand for the atomic radius, electronegativity, and valence electron concentration of element i, respectively; $\bar{r} = \sum c_i r_i$ is the average of atomic radius and $\bar{\chi} = \sum c_i \chi_i$ is the average of the electronegativity; c_i and c_j are the atom fractions of elements i and j; H_{ij} is the enthalpy of mixing of elements i and j at the equimolar concentration in regular binary solutions; $(T_{\mathrm{m}})_i$ is the melting temperature of element i; R is the universal gas constant.[40,65]

Based on this empirical method, it has been suggested that compositional regions of single-phase disordered solid solutions or ordered solid solutions and intermetallic compounds formation can be distinguished by correlating parameters such as δ and ΔH_{mix} or Ω.[40,62–64] Although no correlation was found, considering δ_χ and VEC for a large number of alloys.[40,66] According to Yang and Zhang,[62] when $\Omega < 1$, the enthalpy of mixing is the dominant term in the Gibbs free energy ($\Delta G_{\mathrm{mix}} = \Delta H_{\mathrm{mix}} - T\Delta S_{\mathrm{mix}}$) and therefore tends to stabilize intermetallic compounds, ordered phases, or multiple phases. However, if $\Omega > 1$, the dominant contribution is the entropic one, then there is a tendency of disordered solid solution formation. Moreover, the authors reported a tendency towards single-phase disordered solid solution formation when $\Omega > 1.1$ and $\delta < 6.6\%$. Other attempts, nevertheless, have focused on applying these empirical parameters to distinguish the regions of ordered Laves phase formation. It is especially important since Laves phases present significant potential for structural and functional applications, such as hydrogen storage.[67,68]

The appealing aspect of the empirical approach is its straightforwardness and relative simplicity. Based on parameter calculations, many compositions can be evaluated, and attempts to construct phase stability diagrams can be made.[64] However, the limiting factor of this approach is that it does not consider and compare the formation enthalpies of different possible phases.[51] It is well known that the formation and stability of phases in solids result from the competition among all possible phases in a given thermodynamic state. Thus, the potential of a method to predict phase formation and stability is related to its capacity to account for all competing phases. Furthermore, in the empirical method, the critical values for the parameters (those values meant to indicate the boundaries in the formation of single-phase solid solutions or multi-phase and intermetallics) are arbitrary and back-tested, with insufficient evidence of predictive capacity.[51]

With superior consistency (compared to the empirical approach), thermodynamic models have been able to identify compositional sub-regions where single-phase HEAs exist.[51,69–71] In these approaches, the enthalpies of possible intermetallic compounds are also considered. These thermodynamic models go from the simplest to highly detailed thermodynamic descriptions.[40] Despite their superior thermodynamic coherence, some of these approaches are limited regarding the use of arbitrary values of formation enthalpies of competing compounds.[51] Additionally, as-cast structures (which usually are not the equilibrium ones) are commonly used for experimentally testing and determining the regions of phase formation and stability (as it is in the case of the empirical approach). Finally, sometimes a small effort is employed for determining the reliability of the structural characterization.[40,51]

Another method cited in the investigations of HEAs for hydrogen storage is the Calculated Phase Diagram (CALPHAD).[29,34] This thermodynamic-based method uses computational tools to calculate phase diagrams.[51] The equilibrium-phase diagrams are derived using thermodynamic models that analytically assess the Gibbs–Helmholtz free-energy for all expected competing phases.[51] The thermodynamic models are used in polynomial form, known as Redlich–Kistler functions, and the parameters of the polynomials are fitted by using experimental and theoretical data (that constitute the databases).[51] These databases are built using binary and ternary systems (contributions from higher-order systems are negligibly weak).[40,51] At the moment the free-energy approximations for each of the expected competing phases in an alloy system are identified (as a function of the relevant state variables – usually concentration and temperature at constant pressure), the thermodynamic equilibrium phase for each temperature can be calculated by energy minimization, and the phase diagram is constructed.[51] The reliability of the CALPHAD method is higher when interpolation is done with compositions included in the database.[40] It indicates that extrapolation is generally required in higher-order systems (quaternary, quinary, and so on), potentially reducing the accuracy of CALPHAD predictions.[40]

Nevertheless, extrapolation can give a good predictive capability. It should be mentioned that the first attempt to quantify the accuracy of CALPHAD calculations has already been made.[40] Outside of the ranges fitted by the polynomial functions and when unknown competing intermetallic phases appear, this method currently has limited predictive power.[51] Another limitation is that the CALPHAD method, being based on thermodynamic equilibrium, may miss the prediction of metastable phases that are frequently the phases present in the most successful alloys.[51]

It is a common practice in HEAs studies to investigate the phases predicted by CALPHAD at high temperatures (below the solidus temperature). This region usually favors the stability of solid solutions (if the alloy composition allows) due to temperature contribution in the entropic term of the free energy. It has been reported that these high-temperature phases in HEAs are still present at room temperature (as possibly metastable phases).[29,34,72] Therefore, the CALPHAD method can be helpful as a first approach to exploring the vast compositional space of HEAs.[51]

So far, a few archetypical HEA systems for hydrogen storage have been discovered.[13,22,24,35] Among others, this is the case for the Ti–V–Zr–Nb–Hf system. Since the first report,[13] this system and its derivatives[16,19,22,24,31,32] have been consistently investigated in terms of its hydrogen storage behavior resulting in proposed fundamental mechanisms and properties descriptions.[19,22,24,32] These insights are essential for understanding hydrogen interaction with the hosting metals inside the multi-principal element structures and developing hydrogen storage materials with improved properties. However, compared to the potential number of different systems offered by the HEA approach, there are only a few investigated systems.

As discussed above, among the models for HEA design, the hydrogen storage community has relied mainly on the empirical and CALPHAD methods. Due to its straightforwardness, the empirical method allows the analytical screening of many systems; however, its predictive capacity is limited. The usefulness of this method in finding new promising systems could be improved by using more thermodynamically consistent approaches that consider the enthalpies of the different competing phases.[40,51] Moreover, combinatorial experimental approaches could be linked with the empirical method to assess potential systems better. Combinatorial experiments comprise the fast synthesis and characterization of multiple alloy compositions simultaneously (see this ref. 51 and 'Synthesis and processing methods' section below). As a result, systems that could have the potential for hydrogen storage (estimated based on the calculated parameters) could be fast synthesized and characterized to evaluate their real potential. This approach could help eliminate the non-promising systems and focus on further detailed investigations on the promising ones.

The CALPHAD method is thermodynamically more accurate and presents, in general, broader applicability.[51] As a first attempt to explore the vast compositional space of HEAs, this method can be helpful to find potential systems with broad single-phase fields. However, one has to consider the limits of this approach carefully, especially when it comes to the set of elements present in the systems under consideration since the predictive power of the method is based on the database and not every element or set of elements are assessed (or thoroughly assessed) in these databases.[40] One interesting investigation would be to combine CALPHAD with atomistic models, such as *ab initio* calculations. These atomistic models are not yet developed to assess complex systems but are suited to examine narrow composition ranges that have already been found to be appealing based on another screening technique.[40]

So far, only the desired phase has been considered the primary focus in discussing HEAs design. The influence of the chemical composition on the hydrogen storage properties of the alloy is assumed based on the properties of the hydrides of the respective constituent elements (based mostly on chemical intuition).

Hydrogenation properties-oriented compositional design

The applicability of an alloy as a hydrogen carrier depends mostly on how it interacts with the hydrogen gas. In the following sections, we discuss the theory behind HEA-H interaction (based on thermodynamics) and a few recent attempts to model this interaction (based on thermodynamics and data science).

Thermodynamics of HEA-H systems

The hydrogen storage capacity and the operation temperature–pressure depend on the thermodynamics of hydrogenation/dehydrogenation reactions. Other important properties such as hydrogen absorption/desorption kinetics, cycling stability, reversibility, and material activation and air resistance, are affected by the reaction of the alloy with other reactants (mainly O_2 and H_2O) as well as by kinetics effects (H_2 dissociation and H diffusion, activation energy, *etc.*). However, it is the thermodynamic properties that will determine whether an alloy can absorb hydrogen at a given temperature and pressure and the amount of H in equilibrium within the alloy structure in such conditions. Fortunately, the thermodynamic properties of an alloy are composition-dependent. Therefore, the vast compositional field of HEAs can be used to tune the alloy's thermodynamic properties for different desired applications. Based on this, some fundamental aspects of the thermodynamics of HEA-H systems will be presented.

For any metallurgic system, the equilibrium condition is attained when the chemical potential of all elements in the system are the same in all co-existing phases, resulting in the minimum free energy of the system. When this equilibrium condition is reached, the system is said to be in global equilibrium or ''complete equilibrium'' condition. To achieve complete equilibrium, all atoms of the system must have sufficiently high mobility so the chemical compositions of the phases can be adjusted to minimize the system's free energy. Complete equilibrium can usually be achieved at high temperatures (close to the alloy's solidus temperature). However, in most hydrogen storage applications, the hydrogenation/dehydrogenation reactions occur at low temperatures, way below the alloys' solidus temperature. In this scenario, the mobility of the metal atoms is very limited, and another type of thermodynamic equilibrium may take place, the so-called para-equilibrium (PE). Under PE condition, it can be assumed that the metal atoms are ''frozen'', and only the H atoms are mobile. In this case, an equilibrium condition can also be attained because the H mobility allows the chemical potential of hydrogen to be the same in all the co-existing phases of the

system. Under PE, metal hydrides having the same chemical composition as the host alloy can be formed, and this is what has been reported for most of the HEAs studied for hydrogen storage. Therefore, the thermodynamic description of a single-phase HEA-H system under PE condition will be presented. For a more detailed description of the thermodynamic of systems under complete equilibrium, or other possible equilibrium conditions such as partial or local equilibrium conditions, the readers are encouraged to refer to the fundamental works reported by T. B. Flanagan and W. A. Oates.[73,74]

Here we discuss the investigation of the thermodynamic equilibrium (under PE condition) of a single-phase HEA at a given temperature (T) and a given H_2 pressure (P_{H_2}). The chemical composition of a single-phase HEA can be defined by the atomic fraction of a metal element i, so $\sum c_i = 1$. Because of the PE condition, any possible phase in the system will have the chemical composition fixed in terms of metal elements. Therefore, differences in the chemical composition of the different possible phases are due to the H content in these phases. Thus, it is suitable to define the new chemical variable c_H as eqn (6).

$$c_H = \frac{n_H}{n_M} \tag{6}$$

where n_H is the number of moles of H and n_M is the number of moles of metal atoms in the phase.

Since the chemical composition of the phases in terms of metal atoms are fixed, the equilibrium phases will depend on how the Gibbs free energy of the phase varies with c_H. Therefore, it can be taken as reference state the alloy with its stable structure at that given temperature (it could be BCC, face-centered cubic (FCC), HCP, C14, *etc.*) and the hydrogen gas in its standard condition, *i.e.*, $P^o = 1$ atm. In this case, the change in the Gibbs free energy (ΔG^α) when an H solid solution (α) is formed is given by eqn (7).

$$\Delta G^\alpha(c_H) = G^{MH^\alpha_{c_H}} - G^{alloy} - \frac{c_H}{2}G^{H_2} \tag{7}$$

where $G^{MH^\alpha_{c_H}}$ is the Gibbs free energy of the solid solution α with c_H composition, G^{alloy} is the Gibbs free energy of the alloy in the reference state and G^{H_2} is the Gibbs free energy of the H_2 gas in the standard condition. Note that in this case, the solid solution α has the same structure as the alloy. Fig. 4a schematically shows the variation of ΔG^α as function of c_H for a hypothetical system. Of course, $\Delta G^\alpha(c_H)$ also depends on the chemical composition and crystal structure of the alloy. Under equilibrium, the chemical potential of the elements in the co-existing phases is the same. The H chemical potential of the H_2 gas $\left(\mu_H^{H_2}\right)$ is given by eqn (8) and the H chemical potential in α (μ_H^α) is given by eqn (9).

$$\mu_H^{H_2} = \frac{1}{2}RT\ln\left(\frac{P_{H_2}}{P^o}\right) \tag{8}$$

$$\mu_H^\alpha(c_H) = \frac{d\Delta G^\alpha(c_H)}{dc_H} \tag{9}$$

where R is the universal gas constant. Therefore, the equilibrium H content in the α phase depends on the hydrogen pressure as shown in eqn (10) and Fig. 4b.

$$\frac{1}{2}RT\ln\left(\frac{P_{H_2}}{P^o}\right) = \frac{d\Delta G^\alpha(c_H)}{dc_H} \tag{10}$$

It is worth noting that ΔG^α also depends on the temperature as given by eqn (11).

$$\Delta G^\alpha(c_H) = \Delta H^\alpha(c_H) - T\Delta S^\alpha(c_H) \tag{11}$$

where $\Delta H^\alpha(c_H)$ and $\Delta S^\alpha(c_H)$ are, respectively, the enthalpy and entropy variation between the solid solution α with c_H composition and the reference state. $\Delta H^\alpha(c_H)$ and $\Delta S^\alpha(c_H)$ are defined by eqn (12) and (13), respectively.

$$\Delta H^\alpha(c_H) = H^{MH^\alpha_{c_H}} - H^{alloy} - \frac{c_H}{2}H^{H_2} \tag{12}$$

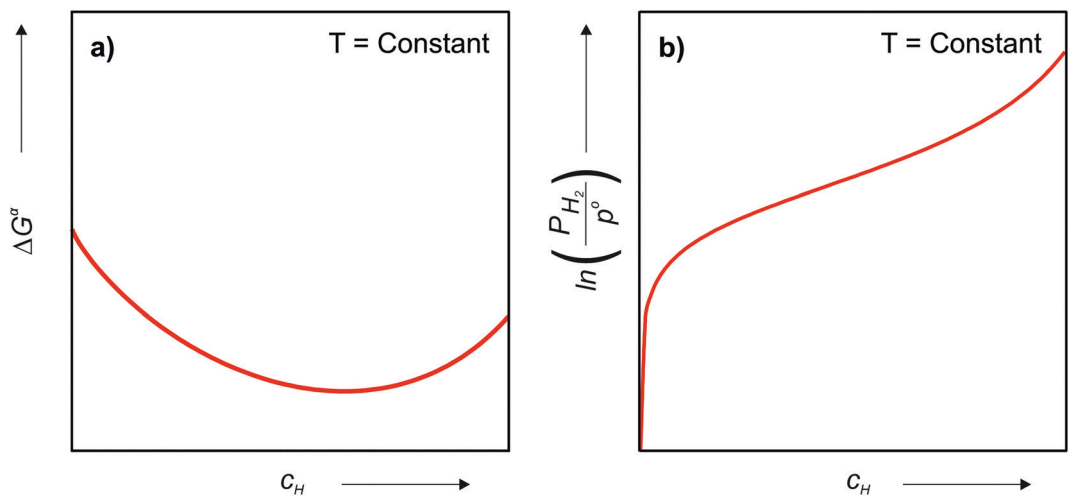

Fig. 4 Schematic representation of (a) Gibbs free energy (b) H_2 equilibrium pressure as a function of the H content in the α-phase for a hypothetical system. The arrows indicate the direction that the values increase.

$$\Delta S^{\alpha}(c_H) = S^{MH^{\alpha}_{c_H}} - S^{alloy} - \frac{c_H}{2}S^{H_2} \quad (13)$$

where $H^{MH^{\alpha}_{c_H}}$ and $S^{MH^{\alpha}_{c_H}}$ are the enthalpy and entropy of the solid solution α with c_H composition; H^{alloy} and S^{alloy} are the enthalpy and entropy of the alloy in the reference state; and H^{H_2} and S^{H_2} are the standard enthalpy and standard entropy of the H_2 gas.

Many HEAs present the formation of different high-entropy hydrides, which have the same composition of the alloy in terms of metal elements, but different crystal structures. For instance, most BCC alloys form an FCC or body-centered tetragonal (BCT) – distorted FCC; dihydride with a CaF_2-type structure upon hydrogenation. It is the case of the TiVZrNbHf, TiZrNbHfTa, and TiVNb–(Cr, Co, Ni) alloys.[13,16,23,72,75] Some of these alloys also form intermediate hydrides. A BCT monohydride is formed as an intermediate hydride in the TiZrNbHfTa–H system.[75] In the TiVNbCr–H, TiVNb(Cr, Ni, Co)–H systems, BCC monohydrides are also observed as intermediate phases.[23,76]

Let us assume a hypothetical case in which two different hydrides, namely β and γ, may be formed. Because of the PE condition, both hydrides will have the same chemical composition in terms of metal atoms as the α phase but different structures. Eqn (14) and (15) present the variation of ΔG^{β} and ΔG^{γ} as function of c_H.

$$\Delta G^{\beta}(c_H) = G^{MH^{\beta}_{c_H}} - G^{alloy} - \frac{c_H}{2}G^{H_2} \quad (14)$$

$$\Delta G^{\gamma}(c_H) = G^{MH^{\gamma}_{c_H}} - G^{alloy} - \frac{c_H}{2}G^{H_2} \quad (15)$$

where $G^{MH^{\beta}_{c_H}}$ and $G^{MH^{\gamma}_{c_H}}$ are the Gibbs free energy of the hydrides β and γ with c_H composition, respectively. Again, the $\Delta G^{\beta}(c_H)$ and $\Delta G^{\gamma}(c_H)$ values also depend on the chemical composition of the alloy and crystal structure of the multi-principal element hydrides. In this case, equilibrium is achieved when the chemical potentials of all components are the same in all co-existing phases. The H chemical potential of α, β and γ are given by eqn (9), (16) and (17), respectively:

$$\mu^{\beta}_H(c_H) = \frac{d\Delta G^{\beta}(c_H)}{dc_H} \quad (16)$$

$$\mu^{\gamma}_H(c_H) = \frac{d\Delta G^{\gamma}(c_H)}{dc_H} \quad (17)$$

Because of the PE condition, the metal elements can be considered as a single component (M) and the chemical potential of M in α, β and γ are simply given by eqn (18)–(20), respectively:

$$\mu^{\alpha}_M(c_H) = \Delta G^{\alpha}(c_H) - c_H\mu^{\alpha}_H(c_H) \quad (18)$$

$$\mu^{\beta}_M(c_H) = \Delta G^{\beta}(c_H) - c_H\mu^{\beta}_H(c_H) \quad (19)$$

$$\mu^{\gamma}_M(c_H) = \Delta G^{\gamma}(c_H) - c_H\mu^{\gamma}_H(c_H) \quad (20)$$

Fig. 5a shows the schematic variation of ΔG^{α}, ΔG^{β} and ΔG^{γ} as function of c_H. In this situation, two phases will co-exist with the hydrogen gas only when the H chemical potential of the gas and both phases are the same and when the M chemical potential of both phases is also the same. The compositions of the two phases having the same μ_H and μ_M can be mathematically determined by finding the common tangent between their Gibbs free energy curves, as shown in Fig. 5a. The α phase with composition $c^{\alpha}_{H,plat\,1}$ and the β phase with composition $c^{\beta}_{H,plat\,1}$ have the same μ_H and μ_M. However, both phases will only exist in equilibrium when μ_H of the H_2 gas is also the same. At a given temperature, this is true only at a single pressure called plateau pressure ($P_{plat\,1}$), in which the equilibrium conditions of eqn (21) and (22) are satisfied:

$$\mu^{H_2}_H(P_{plat\,1}) = \mu^{\alpha}_H\left(c^{\alpha}_{H,plat\,1}\right) = \mu^{\beta}_H\left(c^{\beta}_{H,plat\,1}\right) \quad (21)$$

$$\mu^{\alpha}_M(c^{\alpha}_{H,plat\,1}) = \mu^{\beta}_M(c^{\beta}_{H,plat\,1}) \quad (22)$$

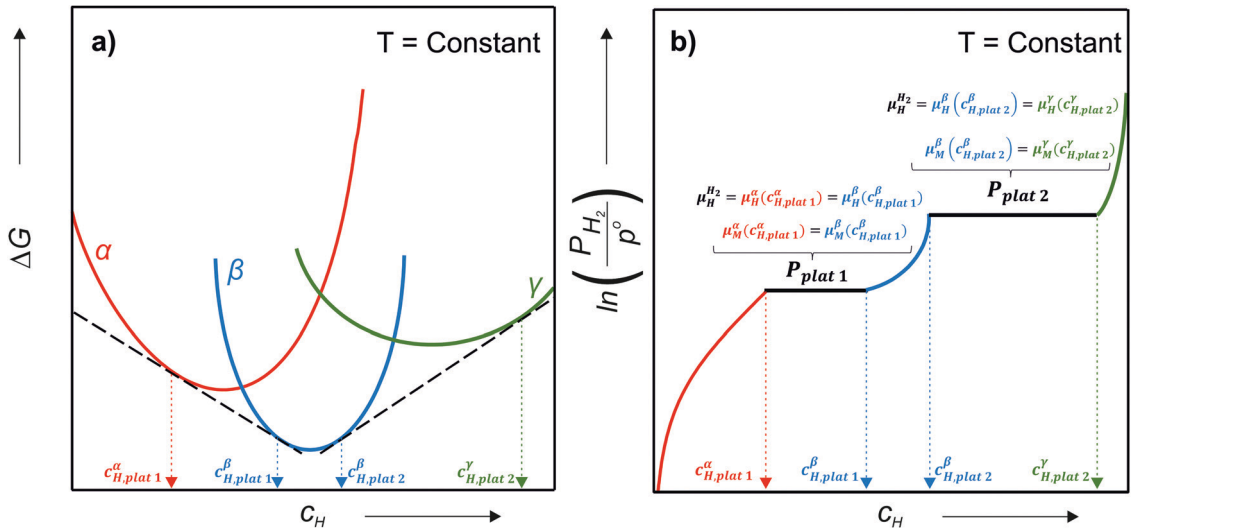

Fig. 5 (a) Schematic curves of ΔG^{α}, ΔG^{β} and ΔG^{γ} as function of C_H at constant temperature and (b) the respective pressure–composition–temperature (PCT) diagram for a hypothetical system. The arrows indicate the direction that the values increase.

In this case, $P_{plat\,1}$ can be determined using eqn (23):

$$\frac{1}{2}RT\ln\left(\frac{P_{plat\,1}}{P^{o}}\right)=\frac{\Delta G^{\beta}\left(c^{\beta}_{H,plat\,1}\right)-\Delta G^{\alpha}\left(c^{\alpha}_{H,plat\,1}\right)}{c^{\beta}_{H,plat\,1}-c^{\alpha}_{H,plat\,1}} \quad (23)$$

Fig. 5a shows that the β phase with composition $c^{\beta}_{H,plat\,2}$ and the γ phase with composition $c^{\gamma}_{H,plat\,2}$ can also exist in equilibrium at a plateau pressure $P_{plat\,2}$ given by eqn (24):

$$\frac{1}{2}RT\ln\left(\frac{P_{plat2}}{P^{o}}\right)=\frac{\Delta G^{\gamma}\left(c^{\gamma}_{H,plat\,2}\right)-\Delta G^{\beta}\left(c^{\beta}_{H,plat\,2}\right)}{c^{\gamma}_{H,plat\,2}-c^{\beta}_{H,plat\,2}} \quad (24)$$

In this case, the equilibrium conditions given by eqn (25) and (26) are satisfied.

$$\mu^{H_2}_{H}(P_{plat\,2})=\mu^{\beta}_{H}\left(c^{\beta}_{H,plat\,2}\right)=\mu^{\gamma}_{H}\left(c^{\gamma}_{H,plat\,2}\right) \quad (25)$$

$$\mu^{\beta}_{M}(c^{\beta}_{H,plat\,2})=\mu^{\gamma}_{M}(c^{\gamma}_{H,plat\,2}) \quad (26)$$

The PCT diagram for this hypothetical system is presented in Fig. 5b. Below $P_{plat\,1}$, only the α phase is in equilibrium with the H_2 gas, and the H content of the α phase depends on the H_2 pressure. At $P_{plat\,1}$, α with $c^{\alpha}_{H,plat\,1}$ composition and β with $c^{\beta}_{H,plat\,1}$ composition co-exist in equilibrium with the gas. Between $P_{plat\,1}$ and $P_{plat\,2}$ only the β phase is in equilibrium with the gas, and its H content also depends on the H_2 pressure. At $P_{plat\,2}$, the β and γ phases with $c^{\beta}_{H,plat\,2}$ and $c^{\gamma}_{H,plat\,2}$ compositions, respectively, co-exist in equilibrium with the gas. Finally, above $P_{plat\,2}$ only the γ phase is in equilibrium with the gas, and its H content also depends on the H_2 pressure. It is worth remembering that ΔG^{β} and ΔG^{γ} is also T dependent as given by eqn (27) and (28).

$$\Delta G^{\beta}(c_H)=\Delta H^{\beta}(c_H)-T\Delta S^{\beta}(c_H) \quad (27)$$

$$\Delta G^{\gamma}(c_H)=\Delta H^{\gamma}(c_H)-T\Delta S^{\gamma}(c_H) \quad (28)$$

where $\Delta H^{\beta}(c_H)$ and $\Delta H^{\gamma}(c_H)$ are the enthalpy variation between the β and γ phases with c_H composition and the reference state, respectively; and $\Delta S^{\beta}(c_H)$ and $\Delta S^{\gamma}(c_H)$ are the entropy variation between the β and γ phases with c_H composition and the reference state, respectively.

Modeling and perspectives on hydrogenation properties-oriented compositional design

In a recent paper, Zepon *et al.*[58] reported on the development of a thermodynamic model for calculating the PCT diagram of multi-principal element M–H systems. As a first approach, the model has been developed for BCC forming alloys, although, according to the work, different structures can also be considered. In this model, the entropy of the phases was described using an ideal configurational entropy for interstitial solid solutions with the site blocking effect model proposed by J. Garcés.[77] As an approximation, it was assumed that the hydrogen partial molar enthalpy of a phase is constant. In addition, the hydrogen partial enthalpy of a multi-principal element phase was calculated (also as an approximation) using a simple ideal mixture law considering the alloy's composition with the same structure of the considered phase. Experimental data for simple hydrides and DFT calculations were used for parametrization of the enthalpy terms. Fig. 6 shows the comparison between the experimental and calculated PCT diagram of the $(TiVNb)_{85}Cr_{15}$ alloy. As reported by Silva *et al.*,[72] this alloy presents two plateaus. The first at low hydrogen pressure between the BCC solid solution (α-phase) and an intermediate hydride (β-phase) which also have BCC structure but with higher hydrogen concentration. This first plateau is described as a hydrogen miscibility gap of the $(TiVNb)_{85}Cr_{15}$ alloy. Because of the gauge pressure's detection limit, the plateau pressure of the α–β equilibrium could not be experimentally determined. A second plateau between the β-phase and an FCC hydride (γ-phase) is experimentally observed at higher pressures. The experimental PCT presents slight sloppy β–γ plateaus with one order of magnitude hysteresis. Sloppy plateaus and hysteresis (*i.e.*, the plateau pressure measured upon absorption is higher than the actual one, and the plateau pressure measured during desorption is lower than the actual) are very common in metal hydrides. Hysteresis is usually attributed to the elastic or plastic accommodation of the volume change (approximately 10 to 20%) during hydride formation and decomposition.[78–82] However, hysteresis can be affected by many factors such as alloy composition, temperature, hydrogen aliquot size, annealing of the metal sample, absorption/desorption cycling, and particle size. All these effects were analyzed in the critical review reported by S. Quian and D. O. Northwood.[82] A systematic study of hysteresis in HEAs is still lacking in literature. Sloppy plateaus can also be

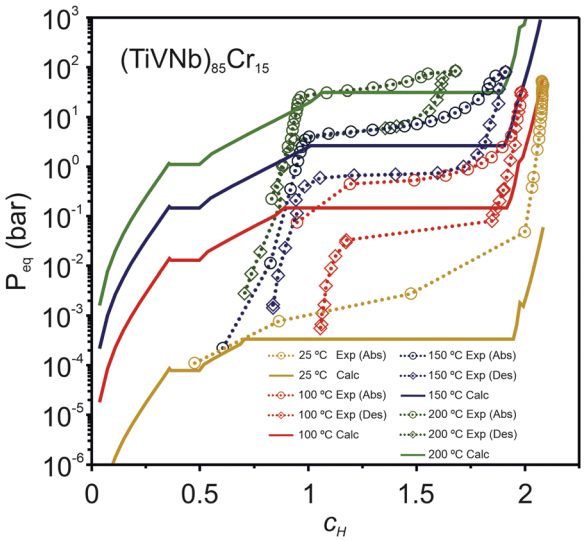

Fig. 6 Experimental PCTs of the $(TiVNb)_{85}Cr_{15}$ alloy measured at 25 °C (298 K) (only absorption), 100 °C (373 K) (absorption and desorption), 150 °C (423 K) (absorption and desorption), and 200 °C (473 K) (absorption and desorption) compared with the calculated PCT using the thermodynamic model proposed by Zepon *et al.*[58] Hysteresis of one order of magnitude is experimentally observed. Reprinted (adapted or reprinted in part) with permission.[58] Copyright 2021, Acta Materialia Inc. Published by Elsevier Ltd.

resulted from elastic or plastic accommodation during hydride formation/decomposition, and from composition gradient within alloy's microstructure. Many HEAs for hydrogen storage are studied in the as-cast condition, and, in these cases, dendritic structures with some level of composition gradient are usually observed. Such composition gradient could lead to sloppy plateaus because of the slightly different equilibrium pressure for regions with different composition. More profound studies on the effect of composition gradient in the shape of PCT diagrams are necessary to elucidate this phenomenon. When no hysteresis and sloppy plateaus are considered in the thermodynamic model (as in the case of the work of Zepon *et al.*[58]), flat absorption and desorption plateaus might present a good predictability of the actual equilibrium plateau pressures. Other quantities that can be used to assess the accuracy of the thermodynamic model are the plateau enthalpy and plateau entropy defined in this case by eqn (29) and (30), respectively.

$$\Delta H_{\text{plat}} = \frac{\Delta H_{\text{m}}^{\gamma}\left(c_{\text{Hplat}}^{\gamma}\right) - \Delta H_{\text{m}}^{\beta}\left(c_{\text{Hplat}}^{\beta}\right)}{c_{\text{Hplat}}^{\delta} - c_{\text{Hplat}}^{\alpha}} \quad (29)$$

$$\Delta S_{\text{plat}} = \frac{\Delta S_{\text{m}}^{\gamma}\left(c_{\text{Hplat}}^{\gamma}\right) - \Delta S_{\text{m}}^{\beta}\left(c_{\text{Hplat}}^{\beta}\right)}{c_{\text{Hplat}}^{\gamma} - c_{\text{Hplat}}^{\beta}} \quad (30)$$

ΔH_{plat} and ΔS_{plat} can be experimentally estimated using the so- called Van't Hoff equation (eqn (31)).

$$\frac{1}{2}\ln\left(P_{\text{plat}}\right) = \frac{\Delta H_{\text{plat}}}{RT} - \frac{\Delta S_{\text{plat}}}{R} \quad (31)$$

In this case, it is assumed that ΔH_{plat} and ΔS_{plat} are constant over temperature (although this is not true, it is a good approximation) and, therefore, these quantities can be found directly by the linearization of $\frac{1}{2}\ln\left(P_{\text{plat}}\right)$ *vs.* $1/T$. For the $(\text{TiVNb})_{85}\text{Cr}_{15}$ alloy, the experimental values of ΔH_{plat} were between −32 and −35 kJ mol^{-1} of H (for absorption and desorption measurements, respectively) and ΔS_{plat} between −83 and −81 J mol^{-1} K^{-1}. For the same alloy, the authors calculated ΔH_{plat} between −32 and −35 kJ mol^{-1} of H and ΔS_{plat} between −75 and −87 J mol^{-1} K^{-1} (the temperature dependencies of ΔH_{plat} and ΔS_{plat} are considered in the model from Zepon *et al.*[58] and these values are those calculated at 25 and 250 °C, respectively). Thus, despite simplifications in the model, the calculated PCT presented very good agreement compared to experimental one. Such good agreement between the calculated and experimental properties was also reported for other alloys of the TiVNbCr and TiVNbNi system. Despite the promising results, the authors recognized that the model needs further improvement since the plateau width (*i.e.*, the difference between the hydrogen concentrations of the two phases in the equilibrium plateau) was not accurately predicted by the model. Moreover, some adjusted parameters for the accurate description of the intermediate hydrides were necessary, still limiting the applicability of the model for high-throughput calculation.

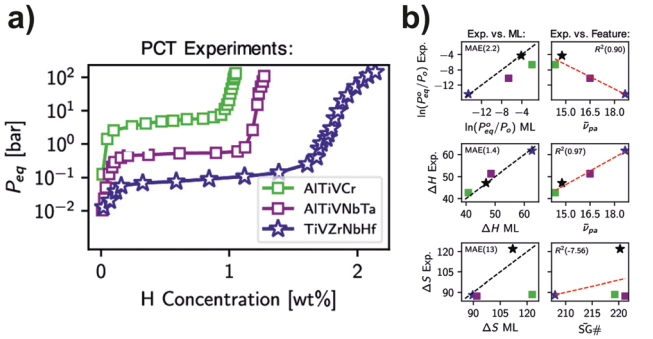

Fig. 7 (a) Experimental PCT isotherms (absorption) at 578, 561, and 571 K for the alloys with compositions TiVZrNbHf, AlTiVNbTa, and AlTiVCr, respectively and (b) experimental hydriding thermodynamic properties compared to ML predictions maintaining the colour references used in (a). The black stars indicate the thermodynamic values for TiVCrNb taken from the PCT data reported in ref. 33. This was included for comparison, considering the central temperature for the Van't Hoff analysis of 100 °C. Reprinted (adapted or reprinted in part) with permission.[57] Copyright 2021, American Chemical Society.

Another approach for calculating thermodynamic properties of HEAs has been reported by Witman *et al.*[57] In this work, the authors used a machine/statistical learning (ML) model to screen the hydride stability of many HEA compositions rapidly. With this model, promising compositions could be down-selected for laboratory validation based on targeted thermodynamic properties. A notable hydride destabilization has been reported *via* using the model for compositional tuning (70 times increase in the equilibrium pressure compared to the benchmark TiVZrNbHfHx HEA hydride) as shown in Fig. 7a. The authors have shown that the method was successful in predicting the destabilization trend in $\ln(P_{\text{eq}}^{0}/P_{0})$ observed experimentally (see Fig. 7b top). Moreover, properties, such as ΔH and ΔS, could also be predicted (Fig. 7b center and bottom, respectively), although it is clear that further improvements are necessary, especially in the calculation of ΔS. It has been indicated that such improvement could come from the utilization of more sophisticated ML methods that take into account specific crystallographic information, relaxation of the assumed temperature independence of ΔS, and the acquisition of more experimental training data. The authors emphasized that better accuracy of the model is expected when more experimental training data become available.

As stated before, the thermodynamic properties of the alloys are composition-dependent, and the vast compositional space of HEA can be explored to design new alloys with tunable properties, *i.e.*, different plateau pressures and H capacities. In addition to the vast compositional space of HEAs, the experimental determination of PCT diagrams is highly time-consuming. Therefore, to be able to efficiently explore a huge number of alloys in terms of their H storage properties, it is paramount to have computational tools to model or predict the thermodynamic properties (P_{eq}, ΔG, ΔH, and ΔS) of the different phases that can be formed in a system as a function of the

alloy composition as well as the H content. Empirical approaches to determine the enthalpy of formation of multi-principal element hydrides using the enthalpies of H solution in the pure elements and the enthalpies of formation of binary hydrides have been used as a guide to design alloys for H storage since the early 1980s.[76,83] Nowadays, the combination of modern computational thermodynamic and machine/statistics learning methods is probably the most appealing way to rapidly explore the thermodynamic properties of a large number of alloys. The models discussed in this work (the thermodynamic model proposed by Zepon *et al.*[58] and the ML model proposed by Witman *et al.*[57]) indicate the potential of this approach (even though further improvements are necessary). ML methods are powerful tools to calculate materials properties and establish relation among them in a big range of compositions. However, they need reliable and extensive enough database to work successfully.[57] In this context, thermodynamic methods could be of great contribution to provide the reliable data that ML methods need. Furthermore, DFT has already been used to determine the enthalpy of formation of single and multi-principal element hydrides through total energy calculations.[18,84–90] Phonon calculations can be used to estimate the temperature dependence of the Gibbs free energy of different phases as a function of composition.[84,88–90] ML has been used to predict the thermodynamic properties of metal hydrides.[91] Although there are still few works that use one or more of these techniques, we suggest that the future of HEA design for hydrogen storage will rely on assessing the thermodynamic properties of different systems through computational methods, which will considerably reduce the number of experiments needed.

Synthesis and processing methods

Most of the HEAs investigated for hydrogen storage are synthesized by arc melting and HEBM (as can be seen in Fig. 8). Moreover, in several other reports LENS,[11,12,14] suction casting,[20,27] melt spinning,[92,93] and HPT[29,34,37] have been reported as used synthesis and processing methods.

Arc melting is an efficient technique in which solid materials are heated *via* an arc plasma created between an electrode and the crucible. In this process, materials can be rapidly heated up to their melting point and then cooled down to room temperature in a short time.[94] This process is commonly conducted in a vacuum or controlled atmosphere that guarantees the synthesis of desired compositions with low contaminants.[95] These aspects combined with this method's straightforwardness may be why the hydrogen storage community has been majorly opting for this synthesis method. Another aspect is that the as-cast structures produced after arc melting reduce the potential difficulties involved in the challenging structural characterization of HEAs since the structures present fewer defects. In general, this could be attributed to different processes that involve melting and solidification compared to processes based on deformation as ball milling, for instance. However, one aspect to consider is that the structures obtained should be carefully evaluated in terms of being the equilibrium

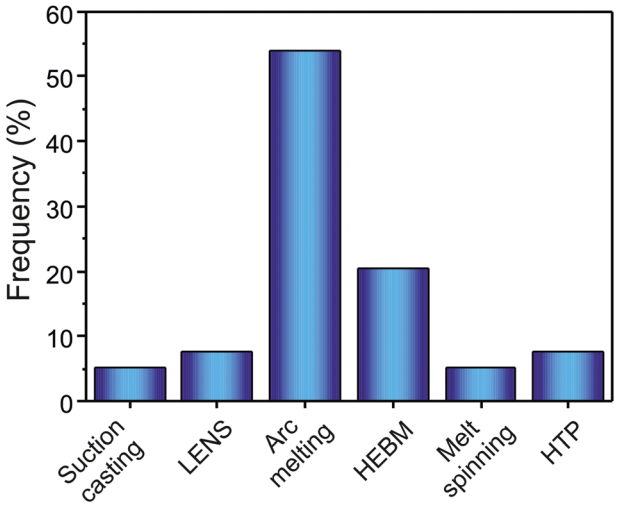

Fig. 8 Frequency of reference of each synthesis and processing method in the HEAs for hydrogen storage literature.

ones, especially when assessing the compositional design method employed is under consideration. As cast structures are usually not the equilibrium ones, and even with following heat treatments after synthesis (with different temperatures and long time), it is not trivial to assure that the equilibrium is reached.[40] However, some procedures can be used to test the stability of the structures synthesized and allow the system to approach the equilibrium. One is to anneal the material at high temperatures near the melting point and for a long time so that sufficient energy and time are available for solid-state diffusion. The system can also approach the equilibrium state by thermo-mechanical processes, such as hot rolling, so that the diffusion constants across the grain boundaries come into play, allowing a faster approximation to the equilibrium. Subsequently, the materials have to be experimentally investigated using spatially resolved elemental analysis for concentration gradients and segregates.[96]

Regarding materials for hydrogen storage, the presence of non-equilibrium structures can limit their applicability since the structure can change during application (*e.g.*, segregation of elements, phase transition), and this can modify the hydrogen storage properties, like the storage capacity, equilibrium pressure, and kinetics. It does not mean that metastable phases (they are stable under certain conditions, but they are not the equilibrium phases) cannot be promising for hydrogen storage, but it is required that the stability of such phases have to be checked under the conditions that the material will be used.

HEBM is a non-equilibrium process that has been used to synthesize different kinds of alloys with refined microstructure (both non-equilibrium and equilibrium phases have been reported after HEBM synthesis). A distinction between mechanical alloying and reactive milling is made in the literature. The first one is a synthesis method where powders of pure elements or pre-alloyed materials are milled under an inert atmosphere. The final product is formed due to repeated cold welding, fracturing, and rewelding.[97] The other one, reactive milling, is

a milling process in a reactive milling environment (for instance, milling under H_2). In this process, besides the alloying of the starting materials, reactions with reactive atmosphere result in products that are the outcome of both phenomena.[97] The hydrogen storage community has used HEBM mainly to synthesize systems containing light elements, especially Mg.[15,22,28,30,35–37] There is no melting process in HEBM; besides, it is suggested that it expands the solubility ranges of the systems, favoring the formation of extended solid solutions.[97] Another promising aspect of milling processes is that they can produce refined microstructures (even down to the nanometer scale), improving the hydrogen storage properties of the materials.[53,97] Despite the advantages, the milling processes may introduce new challenges in the characterization of the synthesized structures due to the creation of various defects.[28,37,97] Furthermore, reproducibility constraints are typical to these processes as the protocols are limited to a set of materials, equipment, and conditions. Besides this, contamination from abrasion of the milling tools and vial is also a concern.[97]

The synthesis and processing methods play an essential role in the investigations and development of new materials, especially in alloys, that can present polymorphism. Moreover, the microstructures can be refined to improve the hydrogen storage properties *via* processing.

As mentioned before, combinatorial method processes may be a promising synthesis and processing route for rapid investigation of new alloy compositions for hydrogen storage. With these processes, portions of alloy's compositional field can be investigated *via* synthesis and subsequent characterization of many alloy compositions simultaneously.[51] Among the techniques of combinatorial processes,[51] combinatorial thin-film materials libraries[98,99] could be a good strategy for the fast identification of potential alloy compositions for hydrogen storage.

BCC HEAs

Metals and alloys with BCC structure have been considered for decades as potential hydrogen storage materials due to the high hydrogen-to-metal ratio (up to H/M = 2). Because of the relatively low molar weight (compared to rare-earth-based compounds), transition-metal-based alloys can absorb gravimetrically large amounts of hydrogen. For example, refractory BCC metals like V absorb up to 4 wt% of H_2.[100] Conventional BCC alloys are mainly based on early 3d transition elements such as Ti, V, Cr, or Fe.[101] It has been shown that the hydrogen storage properties vary greatly depending on the chemical composition of the BCC alloy. For example, the hydrogen storage capacity of 3.67 wt% of H_2 and 2.75 wt% of H_2 were reached by V-rich and Ti-rich BCC alloys, respectively, in the ternary V–Ti–H system.[102]

Recently, it has been suggested that HEAs could show promising hydrogen storage properties as they crystallize in BCC structure. Up to now, the hydrogenation/dehydrogenation properties of dozens of HEAs with different chemical compositions have been studied. The composition of these alloys varies from pure A elements (*i.e.*, elements with high affinity with hydrogen) to materials composed of only B elements (*i.e.*, elements with low affinity with hydrogen). As shown in Fig. 9, most of these alloys are synthesized from 3d and 4d transition metals. The most frequently used elements have been Ti, V, and Zr, which were used in at least 80% of reported HEAs. It should be mentioned that there are a couple of BCC alloys composed mainly of A elements that have been studied in more detail: TiZrNbTa,[20,27,103] TiVZrNb,[21–24,32] and TiVZrHfNb.[13,16,23,24,32,104]

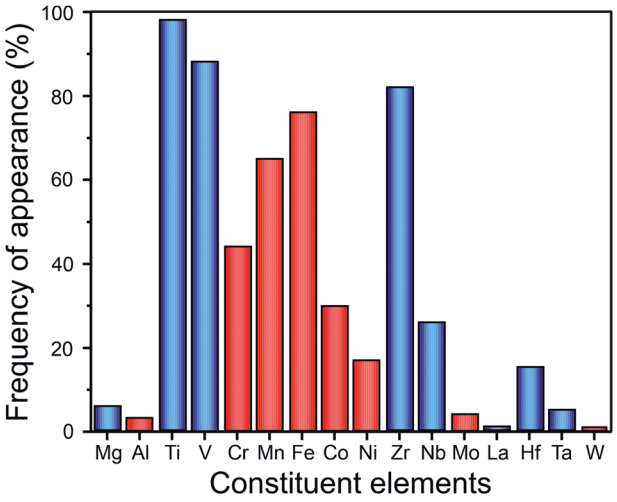

Fig. 9 The frequency with which elements are used in HEAs studied for hydrogen storage. The figure contains data from quinary and senary from all HEA classes. Elements in blue have a high affinity with hydrogen (A elements), and elements in red have a low affinity (B elements).

In the following sections, the aspects related to BCC HEAs for hydrogen storage are discussed considering the alloys reported to date. The summarized features and properties of each of these alloys are shown in Table 1.

Design and synthesis of BCC HEAs

In the last years, many different strategies have been proposed to design and evaluate HEAs with BCC structure for hydrogen storage. For example, Zlotea *et al.*[75] explored the effect of complete substitution of V by Ta on the hydrogen storage properties in the TiVZrNbHf HEA. Surprisingly, the authors have found that the hydrogenated V-free HEA behaves as pure hydrogenated V metal and follows the same phase transformation during hydrogenation. Furthermore, a series of papers investigating the hydrogen storage behavior of BCC HEAs have been published.[13,16,21,23,32] In these papers, a correlation of hydrogen storage properties of the alloys with parameters such as VEC and δ has been proposed. The mentioned relations motivated further investigations. It should also be mentioned that the CALPHAD method has been applied to design BCC HEAs.[72]

In many of the papers reporting HEAs so far, the hydrogen storage performances have been correlated with severe lattice distortion caused by the atomic size mismatch of the elements.

Table 1 Summary of reported BCC HEAs, their characteristics and hydrogen storage performance

Normalized chemical composition ordered by atomic number	Nominal composition	Synthesis and processing	VEC	δ (%)/δ^b (%)	Alloy phase	Hydride phase	Structural transf. upon hydrogenation	H_2 absorp. capacity (wt%)	H/M	Rev. H_2 capacity (wt%/H/M)	H_2 absorp. kinetics	Hydride decompos. onset/peak temperatures (K)	Ref.
$Ti_{0.25}V_{0.25}Cr_{0.25}Nb_{0.25}$	TiVCrNb	Arc melting	5	—/5.69	BCC	FCC(major) BCC(minor)	—	—	~2	1.96 wt% (293 K, vac/ 2.3 MPa H_2) stable 10 cycles	—	473(1.Max) ~556(2.Max)/—	23
$Ti_{0.25}V_{0.25}Cr_{0.25}Nb_{0.25}$	TiVCrNb	Arc melting	5.00	6.18/ 5.69	BCC	BCT/FCC	2 steps	—	~1.9 (373 K)	1.2 (293 K)	—	—/—	33
$Ti_{0.28}V_{0.28}$ $Cr_{0.15}Nb_{0.28}$	$(TiVNb)_{85}Cr_{15}$	Arc melting	4.87	5.85/ 5.16	BCC	FCC	2 steps	3.18 (293 K)	2.0 (293 K)	—	3.18 wt% in 60 s (293 K, 2.5–3 MPa H_2)	324/—	72
$Ti_{0.2}V_{0.2}Cr_{0.2}Nb_{0.2}Mo_{0.2}$	TiVCrNbMo	Arc melting	5.2	—/5.09	BCC	BCC	1 step	—	~1.3	—	—	~523/—	23
$Ti_{0.25}V_{0.25}Cr_{0.25}Mo_{0.25}$	TiVCrMo	Arc melting	5.25	—/4.82	BCC	BCC	1 step	—	~0.75	—	—	~523/—	23
$Ti_{0.2}V_{0.2}Cr_{0.2}Nb_{0.2}Ta_{0.2}$	TiVCrNbTa	Arc melting	5	—/5.52	BCC	FCC(minor) BCC(major)	1 step	—	~1.9	—	—	473 (1.Max) ~556(2.Max)/—	23
$Ti_{0.32}V_{0.32}Co_{0.05}Nb_{0.32}$	$(TiVNb)_{95.3}Co_{4.7}$	Arc melting	4.87	5.02/ 4.33	BCC	FCC	2 steps	3.11 (293 K)	2.0 (293 K)	—	3.11 wt% H/M in 60 s (293 K, 2.5–3 MPa H_2)	362/—	72
$Ti_{0.32}V_{0.32}Ni_{0.04}Nb_{0.32}$	$(TiVNb)_{96.2}Ni_{3.8}$	Arc melting	4.87	4.93/ 4.24	BCC (major) unknown (minor)	FCC	2 steps	3.17 (293 K)	2.0 (293 K)	—	3.17 wt% in 60 s (293 K, 2.5–3 MPa H_2)	409/—	72
$Ti_{0.325}V_{0.275}Zr_{0.125}Nb_{0.275}$	$Ti_{0.325}V_{0.275}Zr_{0.125}Nb_{0.275}$	Arc melting	4.55[a]	—/5.21	BCC	BCT	1 step	2.5 (at 298 K, 5 MPa)	1.75	—	—	~423/ 523(1.Max) 593(2.Max)	22
$Ti_{0.325}V_{0.275}Zr_{0.125}Nb_{0.275}$	$Ti_{0.325}V_{0.275}Zr_{0.125}Nb_{0.275}$	Mechanical alloying (Argon)	4.55[a]	—/5.21	BCC	BCT	1 step	2.5 (523 K, 3 MPa)	1.7	—	—	~473/ 603(1.Max) 703(2.Max)	22
$Ti_{0.325}V_{0.275}Zr_{0.125}Nb_{0.275}$	$Ti_{0.325}V_{0.275}Zr_{0.125}Nb_{0.275}$	Reactive milling (H_2)	4.55[a]	—/5.21	BCC	BCT	1 step	2.7 (293 K, 4 MPa)	1.8	2.0 wt%	—	~458/ 473(1.Max) 523(2.Max)	22
$Ti_{0.25}V_{0.25}Zr_{0.25}Nb_{0.25}$	TiVZrNb	Arc melting	4.50	5.81/ 6.03	BCC	FCC	1 step	—	1.98 (293 K)	—	—	~573/—	32
$Ti_{0.25}V_{0.25}Zr_{0.25}Nb_{0.25}$	TiVZrNb	Arc melting	4.5	—/6.03	BCC	FCC	1 step	—	~2	—	—	553(1.Max) ~648(2.Max)/—	23
$Ti_{0.25}V_{0.25}Zr_{0.25}Nb_{0.25}$	TiVZrNb	Arc melting	4.5[a]	—/6.03	BCC	FCC	1 step (phase separation upon 1 cycle)	—	~1.9	—	—	—	21
$Ti_{0.24}V_{0.24}Zr_{0.28}Nb_{0.24}$	$TiVZr_{1.20}Nb$	Arc melting	4.24[a]	—/6.15	BCC	FCC	1 step (phase separation upon 1 cycle)	—	~1.9	—	—	—	21

Table 1 (*continued*)

Normalized chemical composition ordered by atomic number	Nominal composition	Synthesis and processing	VEC	δ (%)/δ^b (%)	Alloy phase	Hydride phase	Structural transf. upon hydrogenation	H_2 absorp. capacity (wt%)	H/M	Rev. H_2 capacity (wt%/H/M)	H_2 absorp. kinetics	Hydride decompos. onset/peak temperatures (K)	Ref.
$Ti_{0.22}V_{0.22}Zr_{0.33}Nb_{0.22}$	$TiVZr_{1.50}Nb$	Arc melting	4.22[a]	—/6.26	BCC	FCC	1 step (phase separation upon 1 cycle)	—	~1.9	—	—	—	21
$Ti_{0.21}V_{0.21}Zr_{0.37}Nb_{0.21}$	$TiVZr_{1.75}Nb$	Arc melting	4.21[a]	—/6.31	BCC	FCC	1 step (phase separation upon 1 cycle)	—	~1.9	—	—	—	21
$Ti_{0.2}V_{0.2}Zr_{0.4}Nb_{0.2}$	$TiVZr_2Nb$	Arc melting	4.2[a]	—/6.34	BCC	FCC	1 step (phase separation upon 1 cycle)	—	~1.9	—	—	—	21
$Ti_{0.2}V_{0.2}Zr_{0.2}Nb_{0.2}Mo_{0.2}$	TiZrNbMoV	LENS (300 W)	4.8[a]	—/5.77	BCC (major) $NbTi_4$ (minor)	FCC (TiH_x) BCC ($NbH_{0.4}$)	—	2.3 (323 K) 1.78 (after activation 673 K)	—	—	2.3 wt% in 1380 s (303 K, 8.5 MPa H_2)	—	12
$Ti_{0.2}V_{0.2}Zr_{0.2}Nb_{0.2}Mo_{0.2}$	TiZrNbMoV	LENS (1000 W three times)	4.8[a]	—/5.77	BCC (major) Zr-rich (Ppt)	BCC (major) Zr-rich (Ppt)	—	0.59 (323 K) 0.61 (after activation 673 K)	—	—	0.59 wt% in 1380 s (303 K, 8.5 MPa H_2)	—	12
$Ti_{0.22}V_{0.22}Zr_{0.22}Nb_{0.11}Hf_{0.22}$	$TiVZrHfNb_{0.5}$	Arc melting	4.33	6.02/ 6.37	BCC	BCT	—	—	1.82 (293 K)	—	—	~573/—	32
$Ti_{0.22}V_{0.22}Zr_{0.11}Nb_{0.22}Hf_{0.22}$	$TiVZr_{0.5}HfNb$	Arc melting	4.44	5.54/ 5.92	BCC	FCC	—	—	1.99 (293 K)	—	—	~593/—	32
$Ti_{0.22}V_{0.22}Zr_{0.22}Nb_{0.22}Hf_{0.11}$	$TiVZrHf_{0.5}Nb$	Arc melting	4.44	5.80/ 6.10	BCC	FCC	—	—	2.00 (293 K)	—	—	~593/—	32
$Ti_{0.22}V_{0.11}Zr_{0.22}Nb_{0.22}Hf_{0.22}$	$TiV_{0.5}ZrHfNb$	Arc melting	4.33	5.07/ 5.40	BCC	FCC	1 step	—	1.96 (293 K)	—	—	~573/—	32
$Ti_{0.11}V_{0.22}Zr_{0.22}Nb_{0.22}Hf_{0.22}$	$Ti_{0.5}VZrHfNb$	Arc melting	4.44	5.96/ 6.34	BCC	FCC	—	—	1.97 (273 K)	—	—	~573/—	32
$Ti_{0.2}V_{0.2}Zr_{0.2}Nb_{0.2}Hf_{0.2}$	TiVZrHfNb	Arc melting	4.4[a]	—/6.08	BCC	BCT	—	2.1 (573 K) 2.2 (473 K)	1.94 (573 K) 2 (473 K)	—	1.7 wt% in 300 s (573 K, 2 MPa H_2)	623/—	104
$Ti_{0.2}V_{0.2}Zr_{0.2}Nb_{0.2}Hf_{0.2}$	TiVZrHfNb	Arc melting	4.40	5.72/ 6.08	BCC	FCC	1 step	—	1.99 (293 K)	—	—	~593/—	32
$Ti_{0.2}V_{0.2}Zr_{0.2}Nb_{0.2}Hf_{0.2}$	TiVZrNbHf	Arc melting	4.4	6.82/ 6.08	BCC	BCT	1 step	2.7 (573 K)	2.5 (573 K)	—	—	~473/~673	13
$Ti_{0.2}V_{0.2}Zr_{0.2}Nb_{0.2}Hf_{0.2}$	TiVZrNbHf	Arc melting (followed by ball milling)	4.8[a]	—/6.08	BCC	FCC(293 K) BCT(723 K)	1 steps	1.8	1.9 (562 K)	—	—	—	16
$Ti_{0.2}V_{0.2}Zr_{0.2}Nb_{0.2}Hf_{0.2}$	TiVZrNbHf	Arc melting	4.4	—/6.08	BCC	FCC	1 step	—	~1.9	—	—	553(1.Max) ~666(2.Max)/—	23
$Ti_{0.3}V_{0.25}Zr_{0.1}Nb_{0.25}Ta_{0.1}$	$Ti_{0.30}V_{0.25}Zr_{0.10}Nb_{0.25}Ta_{0.10}$	Arc melting	4.6	5.5/ 4.84	BCC	FCC	1 step	2.2 (298 K)	1.73 (298 K)	—	~2.4 wt% in 120 s (373 K, 3.3 Mpa H_2)	~500/ 510(1.Max) 590(2.Max)	31

Table 1 (*continued*)

Normalized chemical composition ordered by atomic number	Nominal composition	Synthesis and processing	VEC	δ (%)/δ^b (%)	Alloy phase	Hydride phase	Structural transf. upon hydrogenation	H_2 absorp. capacity (wt%)	H/M	Rev. H_2 capacity (wt%/H/M)	H_2 absorp. kinetics	Hydride decompos. onset/peak temperatures (K)	Ref.
$Ti_{0.25}V_{0.25}Zr_{0.04}Nb_{0.25}Ta_{0.21}$	$TiVZr_{0.15}NbTa_{0.85}$	Arc melting	4.71[a]	—/4.10	BCC	FCC(major) BCT(minor)	—	—	~1.9	—	—	—	21
$Ti_{0.25}V_{0.25}Zr_{0.125}Nb_{0.25}Ta_{0.125}$	$TiVZr_{0.50}NbTa_{0.50}$	Arc melting	4.63[a]	—/5.09	BCC	FCC(major) BCC(minor	1 step (phase separation upon 1 cycle)	—	~1.9	—	—	—	21
$Ti_{0.25}V_{0.25}Zr_{0.19}Nb_{0.25}Ta_{0.06}$	$TiVZr_{0.74}NbTa_{0.26}$	Arc melting	4.57[a]	—/5.59	BCC	FCC(major) BCC(minor	1 step (phase separation upon 1 cycle)	—	~1.9	—	—	—	21
$Ti_{0.25}V_{0.25}Zr_{0.25}Hf_{0.25}$	TiVZrHf	Arc melting	4.25	6.37/ 6.72	BCC	Phase separation	—	—	—	—	—	—	32
$Ti_{0.25}V_{0.25}Nb_{0.25}Mo_{0.25}$	TiVNbMo	Arc melting	5	—/3.41	BCC	FCC(minor) BCC(major)	1 step	—	~1.5	—	—	473(1.Max) ~556(2.Max)/—	23
$Ti_{0.25}V_{0.25}Nb_{0.25}Hf_{0.25}$	TiVHfNb	Arc melting	4.50	5.12/ 5.56	BCC	FCC	—	—	1.99 (293 K)	—	—	~593/—	32
$Ti_{0.25}V_{0.25}Nb_{0.25}Hf_{0.25}$	TiVNbHf	Arc melting	4.5	—/5.56	BCC	FCC	1 step	—	~2	—	—	553(1.Max) ~648(2.Max)/—	23
$Ti_{0.25}V_{0.25}Nb_{0.25}Ta_{0.25}$	TiVNbTa	Arc melting	4.75[a]	—/3.53	BCC	FCC(major) BCT(minor)	—	—	1.9	—	—	~498/—	21
$Ti_{0.25}V_{0.25}Nb_{0.25}Ta_{0.25}$	TiVNbTa	Arc melting	4.75	—/3.53	BCC	FCC(major) BCC(minor)	1 step	—	~1.9	Fading within 5 cycles to 0 wt%	—	~503(1.Max) ~602(2.Max)/—	23
$Ti_{0.2}Zr_{0.2}Nb_{0.2}Mo_{0.2}Hf_{0.2}$	TiZrHfMoNb	Arc melting	4.6	6.67/ 5.06	BCC	FCC	—	1.18	—	—	—	~540/575	105
$Ti_{0.2}Zr_{0.2}Nb_{0.4}Hf_{0.2}$	$Ti_{0.20}Zr_{0.20}Hf_{0.20}Nb_{0.40}$	Arc melting	4.4[a]	5.51/ 4.01	BCC	FCC	1 step	1.12	—	—	—	656/—	25
$Ti_{0.25}Zr_{0.25}Nb_{0.25}Hf_{0.25}$	TiZrNbHf	Arc melting	4.25	—/4.12	BCC	BCT	1 step	—	~2	—	—	553(1.Max) ~694(2.Max)/—	23
$Ti_{0.25}Zr_{0.25}Nb_{0.25}Hf_{0.25}$	TiZrHfNb	Arc melting	4.25	3.82/ 4.12	BCC	BCT	—	—	1.98 (293 K)	—	—	~623/—	32
$Ti_{0.2}Zr_{0.2}Nb_{0.2}Hf_{0.2}Ta_{0.2}$	TiZrNbHfTa	Arc melting (Homogenized by induction heating)	4.4	4.61/ 4.01	BCC	FCC	2 steps	—	~2.0 (573 K)	—	—	~593/~648	19
$Ti_{0.25}Zr_{0.25}Nb_{0.25}Ta_{0.25}$	TiZrNbTa	Arc melting (followed by suction casting)	4.5	3.75/ 3.86	BCC	Phase separation	2 steps	1.67 (293 K)	—	—	~1.4 wt% in 120 s (293 K, 0.2 MPa H_2)	—	27
$Ti_{0.25}Zr_{0.25}Nb_{0.25}Ta_{0.25}$	TiZrNbTa	Arc melting (followed by suction casting)	4.4	3.75/ 3.86	BCC	—	—	1.4 (300 K)	—	—	~1.4 wt% in 120 s (300 K, 0.2 MPa H_2)	—	20

Table 1 (*continued*)

Normalized chemical composition ordered by atomic number	Nominal composition	Synthesis and processing	VEC	δ (%)/δ^b (%)	Alloy phase	Hydride phase	Structural transf. upon hydrogenation	H_2 absorp. capacity (wt%)	H/M	Rev. H_2 capacity (wt%/H/M)	H_2 absorp. kinetics	Hydride decompos. onset/peak temperatures (K)	Ref.
$Ti_{0.2}Zr_{0.2}Nb_{0.3}Mo_{0.1}Hf_{0.2}$	$Ti_{0.20}Zr_{0.20}Hf_{0.20}Mo_{0.10}Nb_{0.30}$	Arc melting	4.5[a]	6.13/4.59	BCC	FCC	1 step	1.54	—	—	—	605/—	25
$Ti_{0.2}Zr_{0.2}Nb_{0.2}Mo_{0.2}Hf_{0.2}$	$Ti_{0.20}Zr_{0.20}Hf_{0.20}Mo_{0.20}Nb_{0.20}$	Arc melting	4.6[a]	6.67/5.06	BCC	FCC	1 step	1.18	—	—	—	575/—	25
$Ti_{0.2}Zr_{0.2}Nb_{0.1}Mo_{0.3}Hf_{0.2}$	$Ti_{0.20}Zr_{0.20}Hf_{0.20}Mo_{0.30}Nb_{0.10}$	Arc melting	4.7[a]	7.14/5.46	BCC	BCT	1 step	1.40	—	—	—	437/—	25
$Ti_{0.2}Zr_{0.2}Mo_{0.4}Hf_{0.2}$	$Ti_{0.20}Zr_{0.20}Hf_{0.20}Mo_{0.40}$	Arc melting	4.8[a]	7.57/5.80	BCC	BCT	1 step	0.92	—	—	—	441/—	25
$V_{0.25}Zr_{0.25}Nb_{0.25}Hf_{0.25}$	VZrHfNb	Arc melting	4.50	6.22/6.65	BCC (major) unknown (minor)	Phase separation	—	—	—	—	—	—	32
—	$(VFe)_{60}$ $(TiCrCo)_{40-x}Zr_x$	Arc melting (followed by annealing 1673 K for 1800 s)	6.39 (x = 2, stable cyclic performance)[a]	—/5.80 (x = 2)	BCC (major) C14 Laves (minor) CeO_2 (minor) FCC (minor)	—	2 steps	3.5 (298 K)	—	Up to 2.1 wt% (298 K)	3.25–3.5 wt% in 300–600 s (298 K, 4 MPa H_2)	—	101

[a] VEC calculation based on eqn (3). [b] Atomic radii for calculation taken from ref. 106.

δ (atomic size mismatch) is the proposed parameter representing the lattice strain or lattice distortion. X-Ray and neutron total scattering measurements combined with Reverse Monte Carlo structure modeling have shown that larger δ in the Ti–V–Zr–Nb–Hf system corresponds to a higher level of local distortion.[24] Nygard *et al.*[21] have studied a series of HEA compositions to correlate the degree of the local lattice strain with the H/M ratio, but no correlation has been found. Moreover, the same group have shown that the HEA lattice is less prone to strain when smaller elements are embedded in the matrix composed of larger atoms. Therefore, these authors have stated that δ can be misleading in evaluating the local lattice distortion.[33] Notwithstanding, as was suggested by Zlotea *et al.*,[75] larger δ can stabilize a one-phase transformation process during the hydrogenation of BCC HEAs. As presented, no clear overall mechanism has been proposed to link δ with lattice distortion and hydrogen storage behavior, which indicates that more investigations are needed to clarify the usability of δ in designing BCC HEA for hydrogen storage.

The other parameter that has been proposed to describe or predict hydrogen storage properties of BCC HEAs is VEC. It has been shown that the volumetric lattice expansion per atom of hydrogen during hydrogenation increases in a linear function with the increase of VEC (for BCC and HCP structures). Moreover, the larger VEC, the lower is the hydride decomposition onset temperature, and thus the lower thermal stability of the hydride phase.[32] The study of Nygard *et al.*[24] has shown that this effect is also present at the local level. Their study demonstrated that the fraction of occupied interstitial sites with specific nearest-neighbor environments (in the Reverse Monte Carlo structure model of $TiVNbD_{5.7}$) is reduced when the average VEC of the nearest neighbors increases. Moreover, the modeling showed that the size of the tetrahedral interstices does not influence these sites' stability concerning deuterium occupation. It suggests that the stability of the tetrahedral interstices concerning deuterium occupation are directly correlated to the average VEC of the four coordinating metal atoms. Thus, it means that hydrogen is desorbed first from the interstitial sites surrounded by atoms with higher VEC. Moreover, a larger fraction of the interstitial sites are occupied by hydrogen atoms when the VEC of the nearest neighbors is lower (at the local level). It could indicate that lower VEC promotes increased storage capacity. However, in this case, the hydrides' stability is also high, limiting the reversible storage capacity. VEC should be then finely tuned to obtain a good balance between maximum storage capacity and reversible capacity.

It has been suggested that the reversible hydrogen storage capacity can be increased due to destabilization of the hydride phase by fine-tuning the HEA composition.[33] In effect, desorption of hydrogen can start at room temperature when VEC is greater than 6.4.[23] However, considering the reported results, one should keep in mind that the increase of VEC that causes the decrease of hydride phase stability at the same time can reduce the reversible hydrogen storage capacity due to a limitation in the formation of the fully hydrogenated phase (dihydride).

The correlation of VEC with hydrogen storage performance has been further studied by Silva *et al.*,[72] who showed that three Ti–V–Nb-based alloys with the same VEC (4.87) are characterized by similar hydrogen storage capacity and hydrogenation kinetics. Moreover, the authors proposed that VEC can also determine the enthalpy and entropy of hydride formation. However, this has not been confirmed elsewhere yet. The so far published studies indicated that VEC might be an important parameter in BCC HEAs for hydrogen storage and should be taken into account while designing new alloys.

The vast majority of HEAs with BCC structure studied so far have been synthesized by arc melting method (excluding the lightweight alloys described in another section of this review). In few cases, the arc melting has been followed by annealing, suction casting, or ball milling.[16,19,20,27,101] As an example, the $(VFe)_{60}(TiCrCo)_{40-x}Zr_x$ $(0 \leq x \leq 2)$ alloys have been produced by arc melting under Ar atmosphere followed by annealing at 1673 K for 30 min.[101] Moreover, one of the studies presented results for ball-milled HEA (both in Ar and H_2 atmosphere).[22] In another study, Kunce *et al.*[12] used LENS to synthesize the TiZrNbMoV alloy. Different laser energies have been tested in this work, and the respective influence on the microstructure and corresponding hydrogen storage properties was investigated. The authors pointed out that the synthesis methodology still needs to be optimized since the flow of the used powders varies with the morphology of the particles. Thus the obtained chemical composition differs from the nominal content. Moreover, the full interfusion of all elements is possible when high laser power (1000 W) with the repeated melting process is used.

Structure and microstructure of BCC HEAs

The studies described in this section aimed to obtain a single-phase HEA with BCC disordered solid solution. HEAs' structure and chemical composition have been usually evaluated by X-ray diffraction (XRD), selected area electron diffraction (SAED), and Energy Dispersive X-Ray Spectroscopy (EDS). Moreover, the average and local structure of HEAs have also been studied by total scattering measurements and Reverse Monte Carlo structure modeling.[33] As is summarized in Table 1, most of the investigated alloys crystallized in the desired BCC single-phase (the XRD of BCC structure is presented in Fig. 10a). However, in several studies, minor phases or precipitates have also been found.[22,101] For example, $(VFe)_{60}(TiCrCo)_{40-x}Zr_x$ $(0 \leq x \leq 2)$ alloys are composed of the main BCC phase with minor C14-Laves, and Zr-based FCC phases.[101] The investigations of the phase and chemical compositions have shown that the occurrence and abundance of minor phases depend on the chemical composition of the HEA. Nevertheless, it is worth paying attention that the reports on phase formation and stability in HEAs are usually based on as-synthesized structures, which are usually not stable ones in the thermodynamic equilibrium.[40,51] Thus, this should be considered when evaluating these alloys' phase formation and stability. For example, Shen *et al.*,[105] who studied the TiZrHfMoNb alloy, expected the formation of HEA with HCP structure as Ti, Zr, and Hf crystallize in HCP structure. However, as the XRD and SAED results have shown,

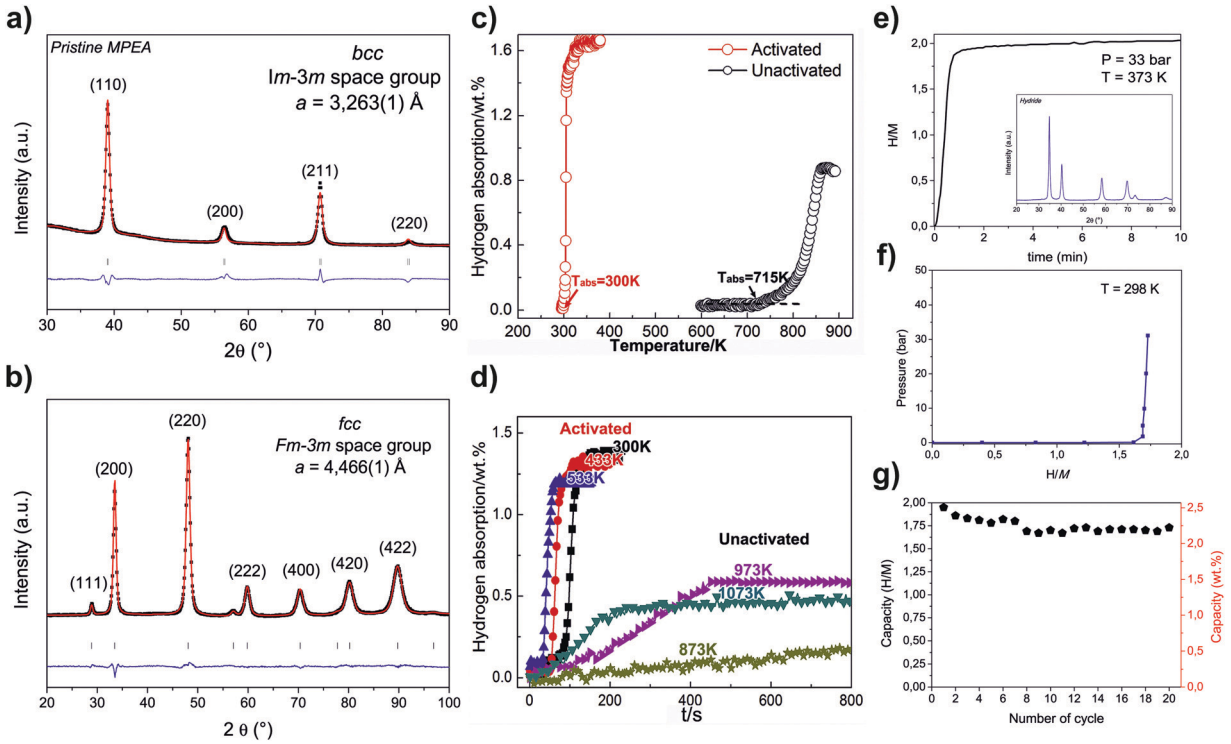

Fig. 10 XRD pattern of as-cast $Ti_{0.30}V_{0.25}Zr_{0.10}Nb_{0.25}Ta_{0.10}$ alloy and related Rietveld refinement analysis (a);[31] *ex situ* neutron diffraction of $Ti_{0.30}V_{0.25}Zr_{0.10}Nb_{0.25}Ta_{0.10}D_2$ and related Rietveld refinement analysis (b);[31] hydrogen absorption in unactivated and activated TiZrNbTa alloy in a function of temperature (heating rate 3 K min^{-1}) (c);[20] kinetics of hydrogen absorption of unactivated and activated TiZrNbTa alloy obtained at different temperatures (0.2 MPa H_2) (d);[20] kinetics of hydrogen absorption in $Ti_{0.30}V_{0.25}Zr_{0.10}Nb_{0.25}Ta_{0.10}$ alloy (373 K, 3.3 MPa H_2) (e);[31] PCT of $Ti_{0.30}V_{0.25}Zr_{0.10}Nb_{0.25}Ta_{0.10}$ alloy obtained at 298 K (f);[31] hydrogen absorption capacity of $Ti_{0.30}V_{0.25}Zr_{0.10}Nb_{0.25}Ta_{0.10}$ upon hydrogen absorption/desorption cycling (g).[31] Reprinted (adapted or reprinted in part) with permission.[20] Copyright 2018, Elsevier B.V. Reprinted (adapted or reprinted in part) with permission.[31] Copyright 2020, Elsevier B.V.

the equiatomic alloy composed of Ti, Zr, Hf, Mo, and Nb resulted in the formation of a BCC structure. In another study, Kunce *et al.*[12] have shown that even though the LENS process used led to inhomogeneities in the composition, an increased laser fluence (1 kW) and threefold remelting led to the formation of a major BCC structure with a residual Zr- and Ti-rich phase. These reports illustrate how the synthesis and processing methods affect the final structures and microstructures of the alloys, which should be taken into account to synthesize stable BCC phases.

Scanning electron microscopy (SEM) with EDS has been used to evaluate the microstructure and homogeneity of HEAs with BCC structure. In most studies, the EDS shows the formation of HEAs with a chemical composition close to the targeted one.[18,27,72,105] Moreover, the EDS mapping commonly suggests a uniform distribution of all elements in the HEA particles at the micrometer level. The homogeneity of the single-phase TiVZrNbHf HEA has been confirmed independently in two papers, with the presence of ~50 μm sized grains.[13,16]

The more detailed studies of arc melted HEAs with BCC structure have revealed a dendritic microstructure in many alloys.[20,21,27,72,103,104] The SEM images combined with EDS analysis of non-equimolar Ti–V–Nb-based and equimolar TiVZrHfNb alloys revealed a gradient of chemical composition between dendritic and interdendritic regions.[72,104] Zhang *et al.* have shown that TiZrNbTa HEA has a dendritic microstructure with a higher concentration of Ta in the dendrites and Ti, Zr, and Nb in the interdendritic sites.[20,103] A comparable dendritic structure has been found by Nygard *et al.*[21] in their systematic study of Ti–V–Zr–Nb–Ta-based HEAs with various degrees of local lattice strain. The study revealed that the microstructure of the as-cast alloys became less dendritic with increasing Zr/M ratio in $TiVZr_zNbTa_{1-z}$ and $TiVZr_{1+z}Nb$ alloys. The dendritic microstructure has also been noticed for HEA synthesized by LENS.[12] The TiZrNbMoV alloy was enriched in Nb and Mo in the dendritic region, while the interdendritic region displayed a large amount of Ti, V, and Zr.[12]

Until now, the microstructure of hydrogenated BCC HEAs has not been studied in detail. The SEM analysis is mainly applied when X-ray diffraction studies show separation or segregation processes after the hydrogen absorption/desorption.[20,103] One of the very few studies has shown (by SEM micrographs) that the hydrogen absorption in TiZrNbTa alloy causes the nanoscale precipitation that forms a lamellar-like microstructure with spinodal-like morphology.[20,103] The study clarified that hydrogen rather than the aging process induced nanoscale phase separation.[20,103] The lamellar structure was further replaced by a spherical shape after hydrogen desorption at 1123 K.[20,103] The size of crystallites for the

TiZrNbTa HEA was revealed in another study and was between 10 and 30 nm.[27,104] In another work, Sleiman *et al.*[104] have shown that after hydrogenation of TiVZrHfNb alloy, a region of the alloy was found in the amorphous state. An amorphous state seems to result from the small particle size and the applied hydrogenation temperature. It should be noted that Zlotea *et al.*[75] proposed the HEA with TiZrNbHfTa composition to check if the obtained BCC alloy would segregate under hydrogenation. The separation process was expected as all these respective elements form stable dihydride phases with FCC structure. However, no segregation has been observed during hydrogen absorption at 573 K under 5 MPa H_2, and a single-phase hydride with FCC structure has been formed.

Hydrogen storage behavior of BCC HEAs

BCC high entropy alloys belong to the most widely studied materials of the HEA class in terms of their chemical composition and hydrogen storage properties, as it is summarized in Table 1. Depending on the chemical composition and applied temperatures, the range of possible gravimetric storage capacities varies from 0.59 wt% to 3.5 wt% H_2. For most alloys, hydrogen-to-metal ratios have been reported close to 2. However, there are exceptions, such as the TiVCrNbMo and TiVCrMo alloys, which achieved H/M ratios of 1.3 and 0.75, respectively.

One of the important functional aspects of HEAs for hydrogen storage is the activation property of the alloys, which is usually related to the material surface area, number of grain boundaries, and surface oxidation state. In most cases, the activation process consists of initial hydrogenation followed by degassing at elevated temperatures under a dynamic vacuum.[21,23,31,32] For example, Ek *et al.*,[32] who studied the arc melted Ti–V–Zr–Nb–Hf system (with ternary, quaternary and quinary compositions), activated most of the materials at 613 K for 3 h under a dynamic vacuum. However, due to very slow absorption kinetics, some of these alloys required elevated degassing temperature (773 K). Sleiman *et al.*[104] studied the effect of the particle size, hydrogenation temperature, and hydrogenation pressure on the activation process of the TiVZrHfNb alloy. This study revealed that the activation properties depend on the particle's size. The reduction of particle size fastens the absorption kinetics and reduces the incubation time. However, at the same time, it negatively affects the maximum hydrogen storage capacity. Similar behavior has been observed by Kunce *et al.*,[12] who observed a reduction of hydrogen storage capacity of TiZrNbMoV alloy from 2.3 wt% to 1.78 wt% of H_2 after activation at 673 K. As was suggested, the reduction of hydrogen uptake is related to the increase of surface/bulk ratio.[104]

The activation of TiZrNbTa has been studied in detail by Zhang *et al.*[20] The studies of hydrogen absorption temperature have shown that the activation process (based on the initial hydrogenation at 0.03 MPa H_2 at 1073 K followed by desorption under vacuum at 1123 K) decreases the hydrogen absorption temperature from 715 K (for inactive material) to 300 K – see Fig. 10c. Moreover, the activation process also promoted hydrogenation's kinetics (Fig. 10d). As X-ray photoelectron spectroscopy (XPS) studies have shown, the activation process causes reduction of the oxides on the HEA surface, firstly to sub-oxides and then to sub-hydroxides. It is noteworthy that this two-step process is unusual for pure metals. The concentration of sub-oxides decreases while sub-hydroxides increases with the cyclic hydrogenation/dehydrogenation process. The authors connected the two-step activation process with the particular interaction among elements incorporated in the HEA. Moreover, the researchers stated that sub-hydroxides rather than sub-oxides are essential to activating the discussed HEA. The proposed rationale is that the H atoms can diffuse through the OH^- group in hydroxides and act as hydrogen diffusion tunnels. Moreover, the mixture of different multi-component sub-hydroxides on the surface can improve the electron transfer between metal and hydrogen ions and generate more interfaces that can act as paths for hydrogen diffusion.[20]

It has been shown elsewhere that the higher Zr-content in $(VFe)_{60}(TiCrCo)_{40-x}Zr_x$ alloys reduces the hydrogenation incubation time. However, it is important to note that the activation of these materials was based only on 30 minutes of degassing of the samples under vacuum at room temperature. It is possible that with proper activation, the problem of incubation for alloys with lower Zr content would disappear. Nevertheless, the incubation time of Zr-free alloy was only 120 s, and taking into account the simplicity of the proposed activation process, these alloys are characterized by excellent activation properties.[101]

The properly-activated HEAs with BCC structure exhibit good hydrogenation kinetics. Ek *et al.*,[32] who have studied a series of ternary, quaternary and quinary alloys from Ti–V–Zr–Nb–Hf system, have shown that most of the materials absorb hydrogen at room temperature within a few hours at 4 MPa of hydrogen. They found out that the presence of V atoms is significant for fast hydrogenation in this system. The deficiency of V causes slower hydrogenation and higher temperatures required for activation.

Sleiman *et al.*[104] have shown that particle size should be considered an essential factor affecting the hydrogenation kinetics. The as-crushed TiVZrHfNb did not absorb hydrogen at 373 K and 473 K even after incubation for 24 h. The alloy started to absorb hydrogen when it was heated to 573 K and 673 K reaching 1.9 wt% H_2 within 100 minutes and 1.9 wt% H_2 within 33 minutes, respectively. The sieving of particles to size lower than 0.5 mm makes the alloy absorb hydrogen below 573 K. At 473 K it absorbs 2.2 wt% (2.0 H/M) with relatively fast kinetics (after 27 h of incubation time).

Other studies have shown that almost full hydrogen storage capacity can be reached even in a minute or second regime. Silva *et al.*[72] have shown that Ti–V–Nb-based alloy can reach the 2 H/M ratio (the equivalent of 3.1–3.2 wt% H_2) in less than one minute at room temperature. The arc melted $Ti_{0.30}V_{0.25}Zr_{10}Nb_{25}Ta_{0.10}$ alloy also absorbs 2 H/M (the equivalent of 2.5 wt% H_2) within two minutes at 373 K under 3.3 MPa of H_2[31] – see Fig. 10e. Furthermore, arc melted TiZrNbTa alloy has reached an equilibrium state during hydrogenation under

0.2 MPa of hydrogen at 293 K within one minute after an incubation time of 150 s. With the increase of temperature, the hydrogenation time can be reduced to 20 s, while the incubation time can be shortened to 35 s. The fitting of kinetic hydrogenation curves has indicated that this process follows the Johnson–Mehl–Avrami equation, which means that the hydrogen absorption in this particular HEA can be described by the nucleation and growth mechanism.[27]

Zhang *et al.*[20] suggested that most of the large vacancy clusters created during hydrogen absorption remain when the hydrogen is desorbed from the structure. Their presence can shorten the diffusion distance of H atoms and, therefore, improve the absorption kinetics. Moreover, these clusters also play an important role in the nucleation process in HEAs. This behavior is different from the one known for AB_5 or AB_2 alloys, and its presence could be explained by the random occupancy of metal atoms in the HEA lattice.

Hydrogen-to-metal ratios higher than 2 have not yet been reported for transition metal elements and alloys, although it is considered that this value could be exceeded.[107] It has been shown that this limit was surpassed in the work of Sahlberg *et al.*[13] The hydrogen absorption measurement revealed an extremely high H/M ratio of 2.5 (the equivalent of 2.7 wt% of H_2) upon hydrogenation at 573 K and 5.3 MPa. This high capacity indicates that hydrogen atoms occupy not only all tetrahedral sites but also some octahedral interstices in the hydride structure (BCT). The corresponding PCT curve has one pressure plateau at 0.01 MPa (H_2) at 573 K, indicating a one-step mechanism in the hydrogenation from BCC to a BCT phase. It is also proposed that the atomic size mismatch of elements forming TiVZrNbHf HEA facilitates significant hydrogen occupation at both sites: octahedral and tetrahedral. However, further studies on the same HEA composition could not reproduce this large H/M ratio. For example, Ek *et al.*[32] measured capacities close to H/M = 2, but no results were shown where H/M of 2 was exceeded. Moreover, no trend has been observed between atomic size mismatch and hydrogen storage properties.

Further investigations by neutron diffraction of deuterated samples have shown that deuterium can occupy both tetrahedral and octahedral interstitial sites in the alloy structure. The distribution of deuterium over the tetrahedral and octahedral interstices has also been evaluated by Reverse Monte Carlo structure modeling for TiVZrNbHf alloy. This study has shown that deuterium tends to avoid occupation of smaller tetrahedral volumes following the Westlake criterion (the interstitial volume should be large enough to accommodate a sphere with a radius of 0.4 Å). Since in HEAs, some sites are smaller than other ones (due to the atomic size mismatch), not all sites meet this criterion. Therefore, it has been shown for this particular HEA that some deuterium can occupy the octahedral sites in place of tetrahedral. The presented distribution shows a partial occupancy of octahedral sites (12%) together with a majority of tetrahedral sites (94%).[24]

The hydrogen occupancy in the structure of different HEAs has also been studied by different groups. Using neutron diffraction experiments on equimolar TiVZrNbHf, deuterium was found to occupy both the tetrahedral and octahedral interstitial sites (at a 53 : 47 proportion) at high temperature and pressure (773 K, 5 MPa D_2). In comparison, the *ex situ* experiments at room temperature showed that the occupation of the tetrahedral sites is preferential (92% tetrahedral occupation, 5.2% octahedral).[16] Similar findings were also reported in the work of Ek *et al.*[32] The diffraction experiments on deuterated TiVZrNbHf-based HEA indicated an increased occupation of the tetrahedral interstices. These observations suggest that the hydrogen occupancy is not limited to the tetrahedral sites, which is also supported by combining theoretical models.

Interestingly, the Reverse Monte Carlo modeling has shown for the not fully deuterated TiVCrNb that hydrogen atoms are mobile between the available sites.[33] On the other hand, in the theoretical work of Hu *et al.*,[108] the absorption behavior of the TiZrHfMoNb alloy was investigated using density functional theory (DFT) calculation. The results indicate that the octahedral sites in the BCC phase are first occupied at low hydrogen concentrations. Above hydrogen content of 1.08 wt% H_2, the BCC structure converts to FCC, and from this point on, the tetrahedral sites of the FCC phase are preferentially occupied. These results are also in good agreement with the observations of Ek *et al.*[32] The diffraction experiments suggest that both interstitials are initially occupied in the BCC phase, with a slight preference toward the octahedral. At high deuterium content, an FCC phase is formed, and the occupation of the tetrahedral interstices dominates. Thus, this mechanism could be attributed to HEAs upon hydrogenation, as it is shown for TiVZrNbHf, $TiV_{0.5}ZrNbHf$, and TiVZrNb alloys absorbing hydrogen with one phase transformation.[32]

Concerning the V–H system, which is of great interest for technical applications due to its high gravimetric storage capacity of $\sim$4 wt% H_2 (H/M = 2) and the possibility of hydrogenation at moderate temperatures and even at room temperature. A disadvantage, however, is that the hydrogenation of vanadium takes place in 2 stages (solid-solution α-phase $\rightarrow$ β-phase (BCT) $\rightarrow$ γ-phase (FCC)), represented by two plateaus in pressure–composition-isotherms. For technical applications, which usually operate at certain working pressure, this could reduce the usable/storable hydrogen quantity by half. Furthermore, for the V–H system, it was found that the hydrogen preferentially occupies the tetrahedral sites in FCC phase of V–H system, as in conventional BCC binary alloys.[109] It is where HEAs become very promising, as their potential compositional diversity allows the respective properties to be fine-tuned and the two-stage absorption process to be bypassed.[13,16,21–23,25,31,32] Accordingly, the non-equimolar $Ti_{0.30}V_{0.25}Zr_{0.10}Nb_{0.25}Ta_{0.10}$ alloy studied by Montero *et al.*[31] shows a single equilibrium pressure plateau below 0.1 MPa at 298 K – see Fig. 10f. The alloy initially present in the BCC phase (see Fig. 10a) exhibits an FCC phase after hydrogenation (see Fig. 10b), which can be identified as the dihydride phase analogous to the fully hydrogenated V–H system. A material with a gravimetric capacity of 2.2 wt% H_2, decreased

thermal stability concerning hydrogenation at room temperature, and increased cycle stability has been obtained.

On the other hand, some HEAs have also been studied, which exhibit two-plateau isotherms. In equimolar Ti–Zr–Nb–Hf–Ta alloy, the pressure–composition–temperature measurements show two-plateau regions, which is characteristic for conventional BCC alloys – with a first plateau corresponding to the formation of a monohydride and the second plateau to the conversion to the dihydride.[75] In addition, the alloys reported by Silva *et al.*[72] ($(TiVNb)_{85}Cr_{15}$; $(TiVNb)_{95.3}Co_{4.7}$; $(TiVNb)_{96.2}Ni_{3.8}$) also presented a two-step hydrogenation process. These findings were supported by X-ray diffraction experiments.[72] Moreover, the hydrogen absorption properties of equimolar TiVCrNb alloy were reported, and the PCT results revealed two plateaus upon hydrogenation and deuteration at temperatures between 373 and 413 K. The arc-melted TiVCrNb shows a BCC structure that transforms to a BCT structure when partially deuterated and to a CaF_2-type structure ($Fm\bar{3}m$) when fully deuterated. These findings were in excellent agreement with the reverse Monte Carlo modeling.[33] However, considering both one-step and two-step hydrogenation, a direct correlation between the chemical nature of the reported HEAs and their hydrogenation-uptake mechanism cannot yet be established. The only explanation has been suggested by Zlotea *et al.*,[19] who have proposed that the character of the phase transition during hydrogenation results from lattice distortion associated with an elemental mismatch in the lattice. The authors proposed that larger δ-values favor a one-step reaction with hydrogen, while the smaller δ-values favor a conventional two-step BCC phase transition.

Furthermore, the question arises which symmetry, BCT or FCC, can describe the dihydride phase and which parameters could be correlated to the respective phase formation. In this regard, Ek *et al.*[32] pointed out that large amounts of Zr and Hf were responsible for forming BCT hydrides rather than FCC. In contrast to the elemental influence of Zr and Hf, this question was also addressed by Nygard *et al.*,[23] who discussed the impact of valence electron concentration. As shown by the authors, HEAs with VEC below 4.4 follow a one-step hydrogen absorption mechanism with a phase transformation from BCC to BCT phase ($I4/mmm$). With increasing VEC ($\geq$4.4), the created metal hydrides crystallize in an FCC phase ($Fm\bar{3}m$). Above 5.2, the BCC structure persists after hydrogenation, and the resulted hydride presents a significantly reduced H/M of 1.3 (compared to those with H/M = 2). However, the studies mentioned above did not clarify if the chemical composition of the HEAs, regardless of VEC, was not the main reason for the reported results.

This topic has been recently addressed by the work of Silva *et al.*[72] In their study, the HEAs with different alloying elements (Cr, Ni, and Co) were designed to have the same VEC of 4.87. The results did not show any significant differences in their hydrogenation properties (the equilibrium plateau pressure, the H/M ratio, the structure of the hydride phase), although the chemical composition of the alloys varied greatly. It suggests that the VEC may have a crucial influence on the corresponding hydride structure whether FCC or BCT is formed. Thus, the properties of solid-state hydrogen storage materials with a BCC structure seem to be strongly dependent on the VEC.

The dehydrogenation process of hydrogenated BCC alloys was investigated using various techniques (differential scanning calorimetry (DSC), thermal gravimetry (TG), temperature desorption spectroscopy (TDS), *in situ* XRD, and neutron diffraction). High desorption temperatures (around 500 K or higher) were reported for most studied BCC HEAs, indicating the presence of stable hydride phases. For example, the hydrogen desorption measurements on TiVZrNbHf showed the desorption onset temperature around 473 K, and the main peak temperature around 673 K.[13] In terms of reduced onset temperature, a significantly better hydrogen desorption behavior was found for Cr-, Co-, or Ni-containing Ti–V–Nb-based alloys. The release of hydrogen from these alloys starts in the range 324–409 K, depending on the chemical composition. The reduced temperature can be attributed to the nature of the elements added, as all three elements poorly form hydrides and are considered B elements. Interestingly, the dehydrogenation onset temperature has been shifted to higher temperatures upon cycling (by 75–120 K). The authors proposed the microstructural changes to explain the mentioned differences in the desorption temperature.[72]

Another approach to destabilize the hydride phase was proposed in Shen *et al.*,[25] where hydrogen storage properties of Ti–Hf–Mo–Nb alloys were investigated. By replacing Nb with Mo and increasing Mo content, the corresponding lattice parameter of the BCC phase and the thermal stability of the hydride phase was decreased. These findings have been further evaluated with theoretical calculations, and it has been proposed that the absolute value of the hydride formation enthalpy decrease with increasing Mo content. Thus, reduced strength of hydrogen-alloy bonding should have reduced the thermal stability. Another interesting finding has been described in the work of Nygard *et al.*,[21] who have shown that Ti–V–Nb–Zr–Ta-based hydrides can be destabilized when the zirconium-to-metal ratio is decreased.

The results of several studies have indicated that some alloys exhibit a more complex hydrogen desorption mechanism.[21,31,32,75] The DSC/TG studies of Ti–V–Zr–Nb–Hf-based HEAs have indicated a hydrogen desorption process following two events. The authors have presented the dehydrogenation onset temperatures in a function of VEC and found that the onset temperature of the first process is relatively stable and is in the range of 573–613 K. In contrast, the second event temperature decreases linearly with increasing VEC. The desorption activation energies obtained from Kissinger plots did not show any systematic correlations with VEC, χ_p, or δ.[32] A very similar behavior in terms of multistage desorption has also been found by Nygard *et al.*,[23] who have studied equimolar ternary, quaternary and quinary alloys with different chemical compositions. However, a clear interpretation of this phenomenon has not been proposed yet. One possible explanation has been proposed by Ek *et al.*,[32] who studied deuterated HEAs and have proposed that the deuterium jumps from tetrahedral sites with high local VEC to octahedral sites with low local VEC during the desorption process causing multistage desorption process. However, experimental evidence for this hypothesis is lacking.

Parallel to the hydrogen desorption mechanism, the phase stability after dehydrogenation should also be considered, as it is crucial for the technical use of the alloys as storage materials. For example, hydrogen desorption in TiVZrNbHf-alloy led to the separation of the previously obtained BCC phase into two BCC phases.[13] Further studies by Nygard *et al.*[24] showed that this separation could be related to the strain in the HEA structure. The researchers assumed that hydrogen absorption relieves some of the strain caused by the different atom sizes. Thus, when hydrogen is desorbed from the metal hydride, the strain increases, and the phase separation might be energetically favored. In addition, the results suggest that metal hydrides formed by Zr- and Hf-containing HEAs have presented phase separation upon the dehydrogenation process.[24] It was also investigated in detail in another work. When HEAs with different zirconium content were examined, phase separation was observed after an absorption/desorption cycle for the samples with zirconium to a metal ratio greater than 0.125. To check the phase stability upon heat treatment, annealing for 24 h in Ar at 1473 K was applied, which did not result in phase separation. It indicates that the observed phase separation was induced by the desorption of hydrogen accommodated in the structure and not by the high temperature.[21]

The studies of the $(VFe)_{60}(TiCrCo)_{40-x}Zr_x$ alloys have also demonstrated that zirconium plays an essential role in hydrogen storage properties. The alloys absorb around 3.5 wt% of H_2 at room temperature while 1.88–2.1 wt% H_2 is reversible. The hydrogen absorption/desorption properties have depended on the phase composition, and it has been shown that the reversible capacity is reduced with greater Zr content. Moreover, the reversible capacity of $(VFe)_{60}(TiCrCo)_{40-x}Zr_x$ was reduced by 4.5–10.9% upon cycling. Furthermore, it was observed that the cycling also caused the reduction of hydrogen desorption plateau pressure. The authors proposed the accumulation of micro-strains as a reason for the deterioration of reversible hydrogen storage capacity.[101]

The cycling behavior of HfNbTiVZr has been extensively studied by *in situ* XRD experiments. The alloy has been systematically tested at different temperatures (573, 673, 773, and 873 K) by alternately applying vacuum during desorption and 10 MPa of hydrogen during absorption processes. The results have shown that the material absorbs hydrogen around 550 K (indicated by phase transformation from BCC to distorted FCC), but the hydride phase remained stable once the vacuum was applied at 573 K. On the other hand, by exposing the hydride phase to vacuum at 673 K, a decrease of the unit cell volume of the distorted FCC structure has been observed. By applying alternating conditions (10 MPa or vacuum at 673 K), the materials response can be considered as ''respiration'' of the material associated with absorption and desorption of hydrogen (correlates with H/M 0.3). If we consider that the fully hydrogenated material shows 1.91 H/M and remains 1.6 H/M under vacuum conditions, it becomes evident that the applied conditions are not sufficient to cause complete desorption. Only cycling at 773 K has caused a reversible phase transformation between BCC (alloy phase) and distorted FCC (hydride phase). After the first cycle, however, the unit cell of the BCC phase remained slightly expanded, for which the authors suggest that either residual hydrogen in the structure or activation of the material may be the causes. These studies illustrate very well that conditions such as temperature and pressure should be chosen carefully when studying the cycling properties of HEAs (to allow complete absorption and desorption of hydrogen).[16]

The slight decrease in the hydrogen storage capacity during the cycling of Ti–V–Nb-based alloys was justified by the increase of defect number (dislocation and grain boundaries), known to diminish the hydrogen storage uptake of metal hydrides. However, the capacity stabilizes after a few cycles, and the level of 88–90% of initial hydrogen storage capacity is retained.[72] Another group has also found decay of the maximum hydrogen capacity with the cycling of $Ti_{0.30}V_{0.25}Zr_{0.10}Nb_{0.25}Ta_{0.10}$ HEA – see Fig. 10g. In this case, the material retained the capacity at a level of 86% of the maximum hydrogen capacity after 20 cycles of hydrogen absorption/desorption. As was shown by SEM images, the deterioration of the capacity did not originate from the phase segregation process. Ultimately, a loss of crystallinity (demonstrated by XRD measurements) was given to reduce hydrogen storage capacity.[31] The loss of crystallinity upon cycling has also been observed for Ti–V–Nb-based alloys.[72]

Zhang *et al.*[27] investigated the cycling properties of TiZrNbTa-alloy and demonstrated that the hydrogen storage capacity is reduced from 1.6 wt% of H_2 to 1.38 wt% of H_2 upon ten cycles. The subsequent SEM images showed a steadily increasing pulverization of the initial particles during cycling, associated with increased defect density due to newly formed grain boundaries. Thus, the results have shown that the capacity decreases, and the incubation time was initially reduced after the first five cycles. Interestingly, however, the incubation time increases again after six cycles, although the particles have been further reduced in size compared to the size measured at the beginning of the study.

Perspectives of BCC HEAs

Considering the research to date, BCC HEAs are promising materials in terms of their hydrogen storage performance. The high hydrogen-to-metal ratio (H/M) of 2.5 reported by Sahlberg *et al.*[13] attracted the attention of the hydrogen storage community. It indicated that HEAs could have superior storage capacity exceeding the hydrogen storage capacity of transition metals and conventional BCC alloys. However, the lack of reports of this phenomenon in other HEA systems indicates that this aspect should be more investigated to consider it a promising feature of HEA compositions. Nevertheless, the reported studies of BCC HEAs have indicated that the hydrogen storage performance of these alloys can be greatly tuned by the chemical composition, resulting in a broad group of materials capable of absorbing hydrogen reversibly both at room and elevated temperatures (see Table 1). Considering the high hydrogen storage capacity (with H/M up to 2) and the vastness of compositions in HEAs, it can reasonably be expected that

BCC HEAs may provide a great opportunity for the development of promising materials for hydrogen storage.

Two promising systems can be highlighted among the alloys studied so far, which form hydrides at room temperature, like the V–H system. The $Ti_{0.325}V_{0.275}Zr_{0.125}Nb_{0.275}$ alloy and the alloys of the TiVCrNb system have shown a reversible storage capacity of 2 wt% of H_2 over several cycles.[22,23] Moreover, the $Ti_{0.325}V_{0.275}Zr_{0.125}Nb_{0.275}$ alloy has been characterized by a single-step transformation during hydrogenation so that the maximum usable hydrogen content is not limited by certain working pressure (considering low-pressure applications, *i.e.*, 0.1–10 MPa), as it is in the V–H system.

Based on the data presented in Table 1, it can be concluded that the majority of the BCC HEAs have been synthesized by arc melting. However, a few reports indicate that other synthesis and processing methods, such as reactive ball milling, can improve hydrogen storage properties.[22] Therefore, further studies on the influence of the synthesis and processing methods on hydrogen storage properties of BCC HEAs are necessary. For example, it is known that by processing, the microstructure of the alloys can be modified and homogenized (removing the dendrites and compositional gradients),[96] which might positively affect the hydrogen storage performance of the alloy.

Little attention has also been paid to the more complex desorption behavior of these alloys. Although many studies reported rapid absorption kinetics, systematic investigation of desorption kinetics is missing. Further studies in this area could contribute to a better understanding of hydrogen desorption from HEAs. Therefore, with the current knowledge, compositions of HEAs could be fine-tuned, and new methods to destabilize the hydride phase could be developed to adjust the decomposition temperatures to the ranges required by different applications.

Moreover, regarding the different mechanisms of HEAs hydrogenation, namely one-stage or two-stage mechanism (or hydrogenation with one or two equilibrium pressures), more systematic studies are necessary since no direct tendency emerges from the work reported so far. It is also worth mentioning the importance of VEC since it has been reported that this parameter has a decisive influence on segregation effects and the decomposition temperature. Therefore, the combination of experimental data and modeling of the respective alloys may be very informative to obtain new insights into the observed phenomena and tendencies.

It is well known that conventional BCCs have a great potential for hydrogen storage. BCC HEAs offer more possibilities for developing promising materials for storing hydrogen due to the vastness of compositions. It is expected that the synthesis of BCC HEAs that store hydrogen reversibly will be significantly facilitated due to the compositional design methods' development. However, the interaction of hydrogen with the hosting alloy structure (at local and bulk level) and the subsequent hydrogen storage properties (*i.e.*, kinetics, cycling, activation) must be further clarified so that the properties of the promising alloys can be enhanced.

Lightweight HEAs

Lightweight solids are considered materials that can reach the United States Department of Energy (DOE) targets for hydrogen storage materials for on-board applications (ultimate system target 6.5 wt% H_2).[110] Therefore, to date, many research groups have extensively studied lightweight materials such as metal–organic frameworks,[111] carbon materials,[112] and lightweight metal hydrides.[5] One of the most promising materials is Mg since it is relatively cheap, light, highly abundant, easy to process, and above all, capable of absorbing hydrogen up to 7.6 wt% H_2. However, the use of Mg for hydrogen storage is restrained because of sluggish hydrogenation/dehydrogenation kinetics, and high temperatures required for hydrogen desorption.[112] For this reason, the search for suitable lightweight hydrogen storage material is still ongoing.

Since Sahlberg *et al.*[13] suggested that HEAs are capable of storing more than two hydrogen atoms over metal atoms (H/M = 2), one of the new ideas for lightweight hydrogen storage materials is to investigate the concept of HEAs consisting partly of light elements incorporated in the solid solution phase. In this way, a high H/M ratio could be kept while the molar mass would be reduced, thereby increasing the gravimetric capacity of the HEA.

Lightweight HEAs have already been studied to evaluate their mechanical properties.[113–115] For example, $Al_{20}Li_{20}Mg_{10}Sc_{20}Ti_{30}$ (32.59 g mol^{-1}, 2.67 g cm^{-3}) with FCC structure has been obtained through the mechanical alloying of elemental powders.[115] The alloy was characterized by very high mechanical hardness – 5.8 GPa (measured with a Vickers indenter). Lightweight HEAs for hydrogen storage have been considered those containing one or more light elements such as Mg, Al, Li. So far, most of the studies on HEA for hydrogen storage have been focused on the transition metals-based alloys with heavy elements from 3d, 4d, and 5d transition groups. As is presented in Fig. 9, the light elements such as Mg and Al have so far been rarely used in HEA for hydrogen storage – in 6.3% and 3.2% alloys, respectively. Moreover, only seven reports have been published, which indicates that this lightweight HEAs field is still undeveloped.

In the following sections, lightweight HEAs for hydrogen storage are discussed considering the studies reported to date. The summarized features and properties of each of these alloys are in Table 2.

Design and synthesis of lightweight HEAs

Up to date, a few lightweight HEAs have been investigated regarding their hydrogen storage properties. Despite the small number of tested systems, the studied alloys cover a very broad range of compositions – from pure A ($Mg_{0.10}Ti_{0.30}V_{0.25}Zr_{0.10}Nb_{0.25}$) through A_2B and $AB_{1.5}$ to pure B alloys (AlCrFeMnNiW). One of the proposed strategies is to study the effect of lightweight elements (Mg) on hydrogen storage properties of already known BCC HEA.[35] However, one challenging aspect of this approach is related to the non-favorable enthalpy of mixing (ΔH_{mix}) among the elements. Taking Mg as an example, it presents positive ΔH_{mix} with some transition metal elements (Mn, Cr, Ti, Nb, for

Table 2 Summary of reported lightweight HEAs, their characteristics and hydrogen storage performance

Normalized chemical composition ordered by atomic number	Nominal composition	Synthesis and processing	VEC[a]	δ[b] (%)	Phases	H_2 storage capacity (wt%)	H/M	H_2 absorp. kinetics	H_2 desorp. kinetics	Enthalpy of hydrogen solution (kJ mol^{-1} H)	Hydride decompos. onset/peak temperatures (K)	Ref.
$Mg_{0.20}Al_{0.20}Ti_{0.20}Fe_{0.20}Ni_{0.20}$	MgAlTiFeNi	Mechanical alloying – Ar – BPR 20 : 1 – RPM 200 – 30 h	5.4	9.24	BCC	—	—	—	—	—		36
$Mg_{0.20}Al_{0.20}Ti_{0.20}Fe_{0.20}Ni_{0.20}$	MgAlTiFeNi	Reactive milling – 3.0 MPa H_2 – BPR 40 : 1 – RPM 600 – 24 h	5.4	9.24	BCC TiH_2 (minor) Mg_2FeH_6 (minor)	1.0 (598 K)	—	1.0 wt% in 3600 s (598 K, 15 MPa)	0.94 wt% in 60 s (598 K, 0.01 MPa)	—	558/598	36
$Mg_{0.20}Al_{0.20}V_{0.20}Cr_{0.20}Ni_{0.20}$	MgVAlCrNi	Mechanical alloying – 0.7 MPa Ar – BPR 20 : 1 – RPM 600	5.2	10.85	BCC	—	—	—	—	—	—	30
$Mg_{0.20}Al_{0.20}V_{0.20}Cr_{0.20}Ni_{0.20}$	MgVAlCrNi	Reactive milling – 3.0 MPa H_2 – BPR 20 : 1 – RPM 600 – 24 h	5.2	10.85	BCC	0.3	0.09–0.14	—	—	+12.2	598/650	30
$Mg_{0.28}Al_{0.19}V_{0.28}Cr_{0.19}Ni_{0.06}$	$Mg_{28}V_{28}Al_{19}Cr_{19}Ni_6$	Reactive milling – 3.0 MPa H_2 – BPR 20 : 1 – RPM 600 – 24 h	4.27	10.07	BCC (major) BCC (minor) MgH_2 (minor)	0.28–0.41 (calc. based on XRD data)	0.11–016	—	—	+9.84	—	30
$Mg_{0.26}Al_{0.31}V_{0.31}Cr_{0.06}Ni_{0.06}$	$Mg_{26}V_{31}Al_{31}Cr_6Ni_6$	Reactive milling – 3.0 MPa H_2 – BPR 20 : 1 – RPM 600 – 24 h	3.81	9.14	BCC (major) BCC (minor) MgH_2 (minor)	—	—	—	—	+8.36	—	30
$Mg_{0.20}Ti_{0.20}V_{0.20}Cr_{0.20}Fe_{0.20}$	MgVTiCrFe	Reactive milling – 3.0 MPa H_2 – BPR 40 : 1 – RPM 600 + HPT	5	8.92	BCC (major) MgH_2 (minor) amorphous phase (minor)	0.3 (623 K)	—	0.2 wt% in 3600 s (303 K, 2 MPa)	—	—	483/520(1.Max) 633(2.Max)	37

Table 2 (*continued*)

Normalized chemical composition ordered by atomic number	Nominal composition	Synthesis and processing	VEC[a]	δ[b] (%)	Phases	H_2 storage capacity (wt%)	H/M	H_2 absorp. kinetics	H_2 desorp. kinetics	Enthalpy of hydrogen solution (kJ mol^{-1} H)	Hydride decom-pos. onset/peak temperatures (K)	Ref.
$Mg_{0.10}Ti_{0.30}V_{0.25}Zr_{0.10}Nb_{0.25}$	$Mg_{0.10}Ti_{0.30}V_{0.25}Zr_{0.10}Nb_{0.25}$	Mechanical alloying – Ar – BPR 26 : 1 – RPM 700 – 2 h	4.3	5.70	BCC	2.7 (298 K)	1.72	2.7 wt% in 60 s (298 K, 2.5 MPa)	—	—	523/563	35
$Mg_{0.10}Ti_{0.30}V_{0.25}Zr_{0.10}Nb_{0.25}$	$Mg_{0.10}Ti_{0.30}V_{0.25}Zr_{0.10}Nb_{0.25}$	Reactive milling – 7.0 MPa H_2 – BPR 60 : 1 – RPM 400 – 1 h	4.3	5.70	FCC	—	1.65	—	—	—	—	35
$Mg_{0.22}Ti_{0.22}Cr_{0.11}Mn_{0.11}Ni_{0.11}Nb_{0.22}$	$MgTiNbCr_{0.5}Mn_{0.5}Ni_{0.5}$	Mechanical alloying – 0.7 MPa Ar – BPR 20 : 1 – RPM 600 – 24 h	5	8.94	BCC (major) Cr (minor) Mn (minor) Mg (minor)	—	0.8	—	—	—	—	28
$Mg_{0.22}Ti_{0.22}Cr_{0.11}Mn_{0.11}Ni_{0.11}Nb_{0.22}$	$MgTiNbCr_{0.5}Mn_{0.5}Ni_{0.5}$	Reactive milling – 3.0 MPa H_2 – BPR 20 : 1 – RPM 600	5	8.94	FCC (major) Cr (minor) Mn (minor) Mn_2NiH_4 (minor)	1.6	—	—	—	—	493/573(1.Max) 653(2.Max)	28
$Mg_{0.22}Ti_{0.22}Fe_{0.11}Co_{0.11}Ni_{0.11}Zr_{0.22}$	$MgZrTiFe_{0.5}Co_{0.5}Ni_{0.5}$	Mechanical alloying – 0.7 MPa Ar – BPR 40 : 1 – RPM 600 – 24 h	5.22	10.31	BCC	1.2 (623 K)	0.67	1.0 wt% in 1800 s (623 K, 2 MPa H_2)	—	−14.4	—	15
$Mg_{0.22}Ti_{0.22}Fe_{0.11}Co_{0.11}Ni_{0.11}Zr_{0.22}$	$MgZrTiFe_{0.5}Co_{0.5}Ni_{0.5}$	Reactive milling – 3.0 MPa H_2 – BPR 40 : 1 – RPM 600 – 24 h	5.22	10.31	FCC	—	—	—	—	—	503/573(1.Max) 648(2.Max)	15
$Al_{0.17}Cr_{0.17}Mn_{0.17}Fe_{0.17}Ni_{0.17}W_{0.17}$	AlCrFeMnNiW	Mechanical alloying – Ar – BPR 10 : 1 – RPM 300 – PCA toluene – 20 h	6.66	9.37	BCC (major) FCC (minor)	0.62 (293 K)	—	—	—	+11	358/—	26

BPR – ball-to-powder weight ratio; RPM – revolutions per minute; PCA – process control agent. [a] VEC calculation based on eqn (3). [b] Atomic radii for calculation taken from ref. 106.

instance), which indicates that the solubility of these elements in a solid solution is limited, as indicated in ref. 28. Therefore, the mixture of Mg with transition metals is not favored, usually resulting in segregation and multiple phases formation.[28,37]

All of the already investigated lightweight HEAs have been synthesized by ball milling techniques since the use of conventional melting techniques is restrained by the low melting temperature of magnesium (923 K), aluminum (933 K), and lithium (453 K). The synthesis of alloys containing Mg by melting processes poses an additional challenge due to the high difference in vapor pressure between the elements (as for Mg with transition metals).[5] Moreover, it has been shown that ball milling is an effective synthesis method of supersaturated solid solutions, and by being so, this method is especially interesting when non-favorable ΔH_{mix} is present.[116] The reports indicate that ball milling techniques are appropriate to synthesize a single-phase lightweight HEA under optimized milling parameters and selected chemical compositions.[15,30,35,36] It should be mentioned that in one of the published works, toluene as a process control agent has been used to prevent cold welding during the milling process.[26] Moreover, to get better activation properties of HEAs, the ball milling process has been supported by high-pressure torsion processing.[37]

Structure and microstructure of lightweight HEAs

Lightweight HEAs for hydrogen storage have been synthesized by ball milling in a protective argon atmosphere and reactive ball milling under a hydrogen atmosphere. Usually, the milling under Ar results in the formation of the solid solution phase (mostly BCC),[15,30,35,36] while milling under H_2 leads to the formation of the hydride phase (mostly FCC)[15,35] – see Fig. 11a and b. However, it is also not uncommon that ball milling of the desired HEA chemical composition ends with the formation of a multiphase alloy.

In one of the first papers published in the field of lightweight HEAs for hydrogen storage, Zepon *et al.*[15] studied the $MgZrTiFe_{0.5}Co_{0.5}Ni_{0.5}$ alloy (A_2B composition) synthesized by ball milling under inert (0.7 MPa Ar) and reactive (3 MPa H_2) atmospheres. The mechanical alloying in Ar resulted in forming a BCC phase with minor unidentified phases. The replacement of Ar by H_2 atmosphere resulted in the formation of the FCC hydride phase. These structures were confirmed by X-ray and electron diffraction techniques. Surprisingly, when the same research group tried to synthesize the equimolar MgVAlCrNi *via* reactive ball milling (at 3 MPa H_2), they obtained BCC structure (instead of the expected FCC hydride phase).[30] As discussed by the mentioned authors, the reason for BCC structure formation is related to the relatively positive enthalpy of hydrogen solution of the selected chemical composition (discussed in detail below). The same structure with a very similar lattice parameter was also obtained when the same mixture of elements was milled under Ar atmosphere.[30] The authors proposed two new non-equiatomic Mg–V–Al–Cr–Ni HEAs. The selected approach was based on the assumption that the increase of Mg and V concentration would decrease the average molar mass compared to equiatomic MgVAlCrNi. Moreover, the change of chemical composition was intended to increase the lattice parameter and, in consequence, increase the solubility of hydrogen into solid solution. However, the synthesis of non-equimolar Mg–V–Al–Cr–Ni HEA by reactive ball milling resulted in the formation of secondary BCC phases and a small fraction of MgH_2 in addition to the main BCC phase.[30]

Dewangan *et al.*[26] also used ball milling under Ar to obtain HEA. X-Ray diffraction studies revealed major BCC and minor FCC structures for AlCrFeMnNiW HEA after milling for 20 h. In another study, a single-phase BCC structure was obtained through ball milling of $Mg_{0.10}Ti_{0.30}V_{0.25}Zr_{0.10}Nb_{0.25}$ chemical composition.[35] Interestingly, MgVAlCrNi HEA crystalizes as a BCC single-phase, although the atomic size mismatch δ (9.7%) significantly exceeds 6.6% – the value proposed by Yang *et al.* as a maximum for creating single-phase alloys.[62] Moreover, a value over 6.6% has been calculated for most of the studied lightweight HEAs (see Table 2). It should be considered another evidence of milling processes' capacity to synthesize supersaturated solid solutions. The BCC single phase has also been found for MgAlTiFeNi HEA milled in Ar.[36] However, the same chemical composition reactively milled under hydrogen pressure (3 MPa H_2) resulted in the formation of multiphase material – with major BCC phase and two minor phases TiH_2 and Mg_2FeH_6.[36]

In another work, $MgTiNbCr_{0.5}Mn_{0.55}Ni_{0.5}$ with a BCC structure was obtained by ball milling under Ar. However, Mg, Cr, and Mn segregation was observed in this synthesis. When the ball-milled alloy was subjected to heat treatment (623 K for 12 h), the segregation of mentioned elements from a BCC solid solution intensified. Furthermore, the reactive ball milling (3 MPa H_2) of the composition mentioned above resulted in the formation of FCC hydride structure and smaller fractions of Cr and Mg_2NiH_4 complex hydride.[28]

De Marco *et al.*[37] processed the reactively milled MgVTiCrFe with high-pressure torsion (HPT). The HPT process resulted in complete amorphization of the material. The hydrogenation studies revealed that HPT could be considered a potential processing method as the obtained alloy was characterized by better hydrogen absorption kinetics than the not-processed sample. However, it should be mentioned that the cyclic hydrogen sorption and desorption in this alloy resulted in material decomposition into less complex compounds (such as TiFe, TiH, $TiCr_2$).

Some of the advantages of mechanical alloying are chemical composition control and nanostructure formation, which favors the hydrogen sorption properties. SEM investigations of reactively milled lightweight HEAs revealed that ball milling techniques promote the formation of particles with 0.5–4 μm (MgVTiCrFe) and 0.5–15 μm (MgVAlCrNi) sizes.[30,37] Further TEM studies showed that the particles are composed of nanocrystallites with size dependent on the chemical composition and vary from 3 to 50 nm.[15,28,30,37] The EDS measurements performed on $MgZrTiFe_{0.5}Co_{0.5}Ni_{0.5}$, $MgTiNbCr_{0.5}Mn_{0.55}Ni_{0.5}$, MgVAlCrNi, and MgVTiCrFe confirmed the homogeneous atomic distribution over the entire materials and creation of

HEAs with a chemical composition close to the designed one.[15,28,30,37]

Hydrogen storage behavior of lightweight HEAs

Most of the lightweight HEAs tested so far can absorb hydrogen only at elevated temperatures. Among the alloys studied, $MgTiNbCr_{0.5}Mn_{0.55}Ni_{0.5}$ (milled under Ar) can absorb hydrogen at 603–723 K, reaching around 0.8 H/M. However, the resulted phase is still a BCC solid solution, and the complete formation of just FCC hydride phase is possible only when reactive milling under hydrogen atmosphere is applied.[28]

The unsatisfactory results of the hydrogenation measurements performed on the equimolar and non-equimolar Mg–V–Al–Cr–Ni HEA (not exceeding 0.15 H/M) prompted the group led by Zepon to search for an explanation. The researchers stated that besides the enthalpy of hydride formation, another factor should be considered to predict hydrogen storage properties of HEAs – enthalpy of hydrogen solution of the alloying elements (the calculated values are presented in Table 2).[30] Their considerations led to the conclusion that lightweight HEAs are even more challenging to design and synthesize since Mg has a very negative enthalpy of MH_2 formation and, at the same time, very positive enthalpy of hydrogen solution.[117] Moreover, for Al, the enthalpy of hydrogen solution is also very positive. Therefore, the diffusion of H atoms into the Mg–Al-containing HEA structures might hardly be hampered.

Much better hydrogen storage properties have been observed for $MgZrTiFe_{0.5}Co_{0.5}Ni_{0.5}$ BCC alloy characterized by the overall negative enthalpy of hydrogen solution (-14.4 kJ mol^{-1} H). The material obtained through ball milling under Ar atmosphere absorbs 1.2 wt% of hydrogen, equivalent to 0.67 H/M (623 K, 2 MPa H_2). The absorption process resulted in the phase transformation to the FCC hydride phase, although this transformation was not complete. The alloy has shown poor kinetic properties under the given conditions, reaching 1 wt% of hydrogen absorption within half an hour.[15]

Recently, $Mg_{0.10}Ti_{0.30}V_{0.25}Zr_{0.10}Nb_{0.25}$ has been studied by Montero *et al.*[35] The hydrogen storage properties of this alloy have been evaluated using Sieverts apparatus. This HEA can extremely fast (in one minute) absorb 2.7 wt% of hydrogen (1.72 H/M) at room temperature – see Fig. 11c. Moreover, the hydrogenation occurs within one phase transformation (from BCC to FCC phase). The cycling capacity is stabilized in one cycle of hydrogenation/dehydrogenation at the level of 2.4 wt% H_2 without any phase separation during repeated hydrogenation/dehydrogenation process.

In the only study showing the hydrogen desorption kinetics, reactively ball-milled MgAlTiFeNi desorbed 100% of the acquired capacity (0.94 wt% H_2) in one minute at 598 K (presented in Fig. 11d). The hydrogen storage capacity of this material has been proven by electrochemical measurements (galvanostatic discharge studies). However, based on XRD,

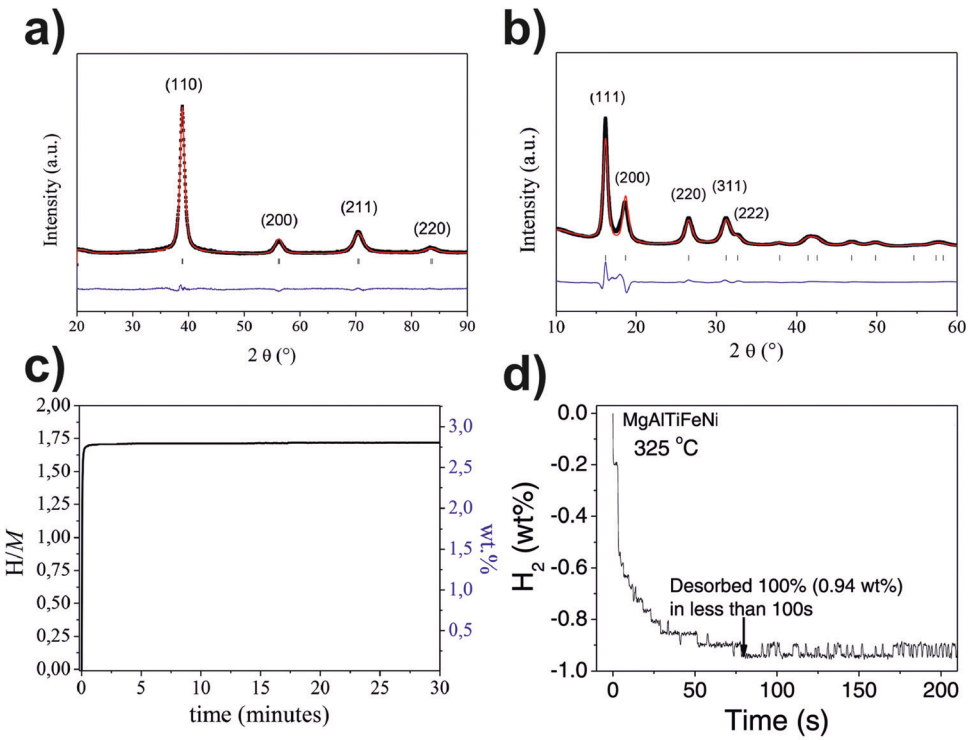

Fig. 11 XRD pattern of the ball-milled $Mg_{0.10}Ti_{0.30}V_{0.25}Zr_{0.10}Nb_{0.25}$ alloy and related Rietveld refinement analysis (a);[35] XRD pattern of $Mg_{0.10}Ti_{0.30}V_{0.25}Zr_{0.10}Nb_{0.25}H_{1.7}$ and related Rietveld refinement analysis (b);[35] kinetics of hydrogen absorption in $Mg_{0.10}Ti_{0.30}V_{0.25}Zr_{0.10}Nb_{0.25}$ alloy (298 K, 2.5 MPa final hydrogen equilibrium pressure) (c);[35] hydrogen desorption from reactively milled MgAlTiFeNi alloy (598 K, 0.01 MPa of hydrogen) (d).[36] Reprinted (adapted or reprinted in part) with permission.[35] Copyright 2021, Acta Materialia Inc. Published by Elsevier Ltd. Reprinted (adapted or reprinted in part) with permission.[36] Copyright 2020, Elsevier B.V.

quadrupole mass spectrometer (QMS), and literature data, the authors stated that this capacity and kinetic properties are probably related to the hydrogen absorption in the minor Mg_2FeH_6 phase rather than to the HEA BCC phase.[36]

The hydride decomposition of lightweight HEAs has been studied by TG, DSC, and TDS. Unfortunately, all of the studied systems are too stable to desorb hydrogen at low temperatures (from 298 to 373 K). As shown by the scientists from ICMPE and Uppsala University, the $Mg_{0.10}Ti_{0.30}V_{0.25}Zr_{0.10}Nb_{0.25}$ alloy desorbs hydrogen at elevated temperature – the process starts around 523 K. Although the authors have stated that hydrogenation/dehydrogenation reactions are completely reversible and occur with single-phase transformation (BCC ↔ FCC), the presented DSC curve indicates the presence of an additional high-temperature decomposition process around 633–643 K.[35] A similar starting hydride decomposition temperature has been observed for $MgZrTiFe_{0.5}Co_{0.5}Ni_{0.5}$ (503 K). This process also consists of two steps- at 573 and 648 K. The dehydrogenation of the hydrogenated sample was further tested by X-ray diffraction studies using a synchrotron light source while raising the temperature.[15] The structure evolution measurements have shown that the first decomposition process is related to the FCC (hydride phase) to BCC (hydrogenated solid solution) phase transition while the second process corresponds to the release of hydrogen from BCC solid solution. A two-step decomposition process has also been observed for reactively milled $MgTiNbCr_{0.5}Mn_{0.55}Ni_{0.5}$ alloy. The first occurs at 573 K and is related to the decomposition of the Mg_2NiH_4 hydride. The other one at 653 K corresponds to hydrogen desorption from the FCC hydride phase.[28] Another material that desorbs hydrogen in two processes is MgTiVCrFe HEA. However, in this case, decomposition steps are related to the multistep decomposition of Mg hydride rather than decomposition of any other phases.[37]

It is noteworthy that Dematteis *et al.*,[118] for the first time, proposed a very interesting approach for hydrogen storage material inspired by the concept of HEA. In this work, a quinary equimolar mixture of light-metals borohydrides ($LiBH_4$–$NaBH_4$–KBH_4–$Mg(BH_4)_2$–$Ca(BH_4)_2$ was reactively ball milled (1 MPa H_2, BPR 30 : 1, 350 rpm, 50 h). This material appears to be promising from the hydrogen release point of view because it is created of multiple cations of light-metals borohydrides characterized by low decomposition temperatures. However, a unique solid solution has not been obtained upon mixing, and some pristine borohydrides are detected in the XRD after milling. Moreover, the hydrogen release temperatures of the obtained multi-phase material are not significantly lowered with respect to those of pure borohydrides. Nevertheless, the proposed concept is very interesting, and a proper way for the synthesis of new solid solutions constituted of five or more borohydrides should be developed.

Perspectives of lightweight HEAs

As it is written at the beginning of this section, to date, the reports on the hydrogen storage performance of lightweight HEAs are limited to seven papers. It seems that the best hydrogen storage performance reported to date has been presented by $Mg_{0.10}Ti_{0.30}V_{0.25}Zr_{0.10}Nb_{0.2}$.[35] So far, this alloy is the only one capable of absorbing a large content of hydrogen (1.7 H/M, 2.7 wt% H_2) at room temperature. Moreover, the hydrogenation process is extremely rapid. Compared to Mg-free $Ti_{0.30}V_{0.25}Zr_{0.10}Nb_{0.2}$ alloy, $Mg_{0.10}Ti_{0.30}V_{0.25}Zr_{0.10}Nb_{0.2}$ alloy absorbs hydrogen around 40 times faster.[35] It shows that lightweight elements could not only increase the gravimetric capacity of HEAs but also significantly improve other hydrogenation properties.

However, it is worth mentioning that the $Mg_{0.10}Ti_{0.30}V_{0.25}Zr_{0.10}Nb_{0.2}$ alloy is composed mainly of transition metals, and the lightweight element constitutes 10% of the alloy composition. The other HEAs analyzed in this section are composed of 17–57% of lightweight elements (Mg, Al). As it was pointed out in ref. 28, the formation of solid solutions (especially single phase) by mixing lightweight elements with transition metals is challenging due to non-favorable enthalpies of mixing, which may limit the concentration of light elements that can be added to these alloy systems.

Most investigated materials cannot absorb or desorb hydrogen at moderate conditions. Their H/M ratio is mostly (with an exception for $Mg_{0.10}Ti_{0.30}V_{0.25}Zr_{0.10}Nb_{0.25}$) far from the value obtained by conventional BCC alloys (H/M = 2) or the value published by Sahlberg *et al.* (H/M = 2.5).[13] Thus, taking into account the reports published to date, these alloys' gravimetric capacities are generally limited by the inability to obtain the dihydride phase. As discussed above, the possible rationale can be related to the positive enthalpy of hydrogen solution of some light elements (Mg, Al) that have to be balanced by other elements with negative enthalpy of hydrogen solution in order to allow hydrogenation o the HEAs. Therefore, the enthalpy of hydrogen solution could be an essential factor to consider in developing lightweight HEAs.

More investigations are required to evaluate the potential of this group of HEAs for hydrogen storage. Moreover, there is limited information about the cyclic hydrogen absorption/desorption performance of lightweight HEAs with a significant content of light elements. Compared to pure Mg, lightweight HEAs have greater molar mass (42.6 g mol^{-1} for MgVAlCrNi and 24.3 g mol^{-1} for Mg), potentially more expensive, and show limited performance under hydrogenation. It has been recently shown that non-confined MgH_2 nanoparticles (4–5 nm) can store 6.7 wt% of H_2 at 303 K and operate cyclically for at least 50 cycles at 423 K.[119] Moreover, the Mg-based alloy with the addition of multiwalled carbon nanotubes absorbs 5.6 wt% of H_2 within one minute at 373 K.[120] These properties are not available for HEA at the current state of knowledge. However, it should be once again emphasized that the studies of lightweight HEA for H_2 storage have just begun, while the Mg-based hydrogen storage systems are probably the most widely studied among all hydrogen storage materials.

In the light of the available reports, it seems that one real merit of lightweight HEAs could be as a potential way to increase the gravimetric capacity of promising transition metal-based alloy systems. However, given the limited number

of reports, it is worth paying attention to the issues related to mixing of higher amounts of light elements (considering the formation of single-phase solid solutions) and achieving a greater degree of hydrogenation (formation of dihydrides, for instance), initially out of scientific curiosity, but with a considerable potential for future applications.

Intermetallic HEAs

Since the discovery of hydrogen absorption in $LaNi_5$ and FeTi, intermetallic compounds have been intensively investigated for hydrogen storage.[2] Usually, an intermetallic compound for hydrogen storage is formed by combining a stable hydride forming element (A elements) with a nonstable hydride forming one (B elements).[2] In the simplest case, a ternary system AB_xHn can be formed by hydrogenation (A are usually rare earth, alkaline earth, or transition metal, and B is often a transition metal). These compounds present well-defined A : B ratios that can form hydrides with a hydrogen-to-metal ratio of up to two.[121] However, for most of the intermetallic compounds investigated so far, their low energy density per unit weight at ambient conditions is a critical disadvantage.[2]

$LaNi_5$ is a representative of AB_5-type alloys, and it was extensively investigated for hydrogen storage due to its capability of working in moderate conditions, besides presenting low hysteresis and flat plateaus in the PCT diagrams.[2,122,123] The investigation efforts have focused on improving the reversible capacity, cycling capacity, kinetics, and impurity resistance. AB-type alloys are another group that has been extensively studied. TiFe is the main representative of these alloys, presenting a storage capacity of 1.90 wt% H_2 with inexpensive elements.[2] The main drawback of this compound is the necessity of its inconvenient activation process that requires high pressure and temperature.[2,124,125] Another important group of alloys is the AB_2-type. These alloys usually form Laves phase, and the most prominent alloys from this group are those with Ti and Zr on the A site.[2] Laves phase structures present good hydrogen storage capacity, fast kinetics, long cycling life, and relatively low-cost materials.[2,126] Some of these alloys form stable hydrides at room temperature (they have low equilibrium pressures at room temperature).[124] However, due to the great properties tuning possibility *via* elemental modification, hydride destabilization has been successfully achieved.[127] A couple of AB_2-type alloys form unstable hydrides (hydrides that present high equilibrium pressures at room temperature), which have been investigated for the hybrid hydrogen storage concept (in which hydrogen is stored as pressurized gas and in the hydride).[45,128,129]

One interesting approach that has been investigated for improving the properties of these alloys (especially AB_2-type alloys) is the introduction of disorder in the Laves structure *via*

Table 3 Summary of reported intermetallic HEAs, their characteristics and hydrogen storage performance

Normalized chemical composition ordered by atomic number	Chemical composition	Synthesis method	Alloy phase	VEC	Maximum H_2 storage capacity (wt% H_2)	H_2 absorption kinetics	H/M	Hydride decomposition temperature (K)	Ref.
$Ti_xV_yCr_uMn_wFe_vZr_z$	$Cr_uFe_vMn_wTi_xV_yZr_z$ $0 \le u, v, w, x, y, z \le 2$	Arc melting	C14 Laves	—	0.55–2.23	$19 \le t_{0.9}$ (s) ≤ 84 (298 K, 0.98 MPa H_2)	—	278, 298, 353[ac] >573 (DSC)	17
$Ti_{0.17}V_{0.17}Cr_{0.17}Fe_{0.17}Ni_{0.17}Zr_{0.17}$	ZrTiVCrFeNi	LENS	C14 Laves (major) α-Ti solid solution (minor)	6.17[b]	1.81	—	—	323[a]	11
$Ti_{0.17}V_{0.17}Cr_{0.17}Fe_{0.17}Ni_{0.17}Zr_{0.17}$	ZrTiVNiCrFe	Arc melting	C14 Laves	6.17[b]	1.3–1.6	—	—	308[ac]	92
$Ti_xV_yMnFeCoZr_z$	CoFeMnTi$_x$V$_y$Zr$_z$ $0.5 \le x \le 2.5$; $0.4 \le y \le 3.0$; $0.4 \le z \le 3.0$	Arc melting	C14 Laves	—	0.03–1.80	$18 \le t_{0.9}$ (s) $\le$ 1250 (298 K, 0.97 MPa H_2)	0.02–1.17	298[a]	10
$Ti_{0.17}Cr_{0.17}Mn_{0.17}Fe_{0.17}Ni_{0.17}Zr_{0.17}$	TiZrCrMnFeNi	Arc melting + HPT	C14 Laves (major)	6.4	1.7	1.6 wt% H_2 in 60 s (303 K, 3.9 MPa H_2)	1	305[a]	29
$Ti_{0.20}Fe_{0.40}Ni_{0.15}Zr_{0.20}Nb_{0.05}$	$Ti_{20}Zr_{20}Nb_5Fe_{40}Ni_{15}$	Arc melting	C14 Laves (major) BCC (minor)	6.5	1.38	—	0.95	305[ac]	34
$Ti_{0.20}Fe_{0.20}Ni_{0.20}Zr_{0.20}Nb_{0.20}$	TiZrNbFeNi	Arc melting	C14 Laves (major) BCC (minor)	6.2	1.64	—	1.17	305[ac]	34
$V_{0.20}Mn_{0.20}Fe_{0.20}Ni_{0.20}La_{0.20}$	LaNiFeVMn	LENS	Multiphase	—	0.3–0.83	0.13–0.83 wt% H_2 in 600 s (308 K, 4.5 MPa H_2)	—	308[a]	14

$t_{0.9}$ – time for reaching 90% of the maximum capacity (in seconds). [a] Desorption performed in a Sieverts-type apparatus. [b] VEC calculation based on eqn (3). [c] Not fully dehydrogenated (retained H_2 in material).

using excess elements and non-stoichiometric compositions.[130] In this regard, the HEA concept may offer a promising opportunity since the use of multi-principal elements may generate disorder in these structures,[40] resulting in improved hydrogen storage properties. Besides that, the use of multi-principal elements greatly increases the possibility of combinations for developing materials with improved properties (the main appealing aspect of the HEA concept).

In the following sections, the aspects related to intermetallic HEAs for hydrogen storage will be discussed, considering the set of reported compositions as a whole. To look at the features and performance of particular alloys, refer to Table 3.

Design and synthesis of intermetallic HEAs

As has been mentioned previously, the most prominent Laves phase alloys for hydrogen storage possess Ti and Zr in their composition. Accordingly, in the design of new Laves phase forming HEA systems, these elements have received most of the attention, and other transition metals (mainly V, Cr, Mn, Fe, and Co) have been used to compose the multi-principal element systems.

Most of the reported compositions are equiatomic.[11,29,34,92] However, attempts have been made to understand how the hydrogen storage properties change among different compositions within the same alloy system.[10,17] The results shown in one of the reports indicate that for some systems, improved hydrogen storage behavior can be found in non-equiatomic compositions.[34] The empirical and CALPHAD methods have been cited as methods that guided the design of these alloys.[11,29,34] As for disordered solid solution alloys (such as BCC HEAs analyzed in the previous sections), the formation and stability of intermetallic HEAs (especially Laves phase forming HEAs) have been related to empirical parameters, like δ and VEC, and thermodynamic variables like ΔH_{mix}, as can be seen in ref. 67 and 68. In spite of this, no clear general criterion for the formation of intermetallic HEAs is available yet. Arc melting has been mainly used to synthesize these materials.[10,17,29,34,92] It should also be pointed out that no intermetallic HEAs for hydrogen storage have been synthesized by ball milling methods.

Structure and microstructure of intermetallic HEAs

Kao *et al.*[10] systematically investigated the $CoFeMnTi_xV_yZr_z$ alloy system. After synthesis *via* vacuum arc melting, all the investigated chemical compositions presented a single C14 Laves phase (based only on XRD analysis), despite the wide range of x, y, and z (molar fraction) used in the systematic study. Upon hydrogenation, the alloys have remained C14 Laves structure (no indication of phase separation has been observed), and the H_2 uptake leads to expansion of the structure, as determined *via* XRD. Another systematic study was conducted by Chen *et al.*[17] In this work, alloys of the $Cr_uFe_vMn_wTi_xV_yZr_z$ system were also produced by arc melting, presenting a main C14 Laves structure. This structure has been maintained after the hydrogenation process. La–Ni–Fe–V–Mn alloy system has also been systematically investigated, but in this case, a more complex microstructure was obtained, causing difficulties in analyzing the hydrogen storage behavior of these alloys.[14] Kunce *et al.*[11] reported that ZrTiVCrFeNi composition presented a dominant C14 Laves phase matrix with α-Ti solid solution secondary phase. After synthesis by LENS and annealing at 1273 K for 24 h, it was shown that the microstructure was composed of three chemically different areas. Moreover, the lattice parameters of the C14 Laves phase have changed slightly during heat treatment. This change in the lattice could be associated with a relaxation of internal lattice strain and diffusion of elements.

Edalati *et al.*[29] and Floriano *et al.*[34] reported the compositional optimization of different alloy systems (towards single-phase formation) using the CALPHAD method. The former authors calculated that the TiZrCrMnFeNi composition should present a high single-phase field in the equilibrium (in contrast to the multi-phase forming TiVCrMnFeCo composition). After synthesis by arc melting, it was verified that the structure of the TiZrCrMnFeNi was composed by a main C14 Laves phase along with small fractions of secondary Ti- and Ni-rich cubic phase (measured by EDS elemental mapping).[29] The latter authors reported the compositional optimization (towards single phase formation) within the same TiZrNbFeNi alloy system. It was shown that, although the equiatomic and the non-equiatomic ($Ti_{20}Zr_{20}Nb_5Fe_{40}Ni_{15}$) compositions present more than one phase, the non-equiatomic one has fewer amount of secondary phases. SEM-EDS results indicated a good level of homogeneity in both compositions. However, the non-equiatomic one presented an evident chemical gradient (seen in the EDS mapping).[34] Zadorozhnyy and co-workers investigated the CoFeMnTiVZr and ZrTiVNiCrFe compositions for hydrogen storage by electrochemical and gas-solid reactions. Both compositions were processed by melt spinning and were characterized by single-phase C14 Laves structure.[92,93]

Hydrogen storage behavior of intermetallic HEAs

As shown in Table 3, the maximum hydrogen storage capacity of the alloys investigated so far is in the range of 0.03 to 2.23 wt% H_2. In terms of H/M, the reported values are between 0.02 and 1.17. Most of the investigated alloys present fast kinetics. However, one common issue reported in the papers is that segregation of some elements (Ti, Zr) might deteriorate the absorption capacity of these alloys due to the reduction of regions prone to hydrogen absorption (the segregated elements can easily form oxides). Furthermore, due to the high affinity of some elements to hydrogen (elements that present high enthalpies of hydride formation), hydrogen can be retained in the structure of HEAs after absorption/desorption cycles which limit the reversible capacity of these alloys considerably.[10,11] The reported investigations showed that these alloys' hydrogen storage behavior and properties could be extensively tuned *via* chemical composition modification.[10,17] These effects are associated with different interactions of hydrogen in the structure (chemical interaction aspect) and the volume of the interstitial sites (which is also a function of the chemical composition).[10,17,34] In this regard, it is reported that

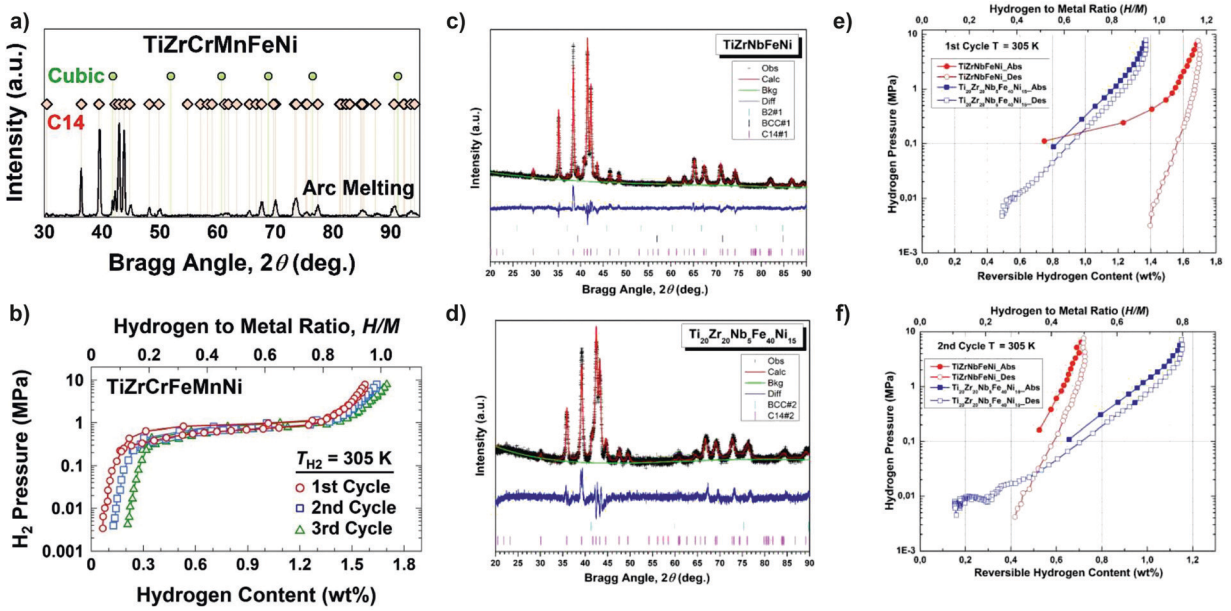

Fig. 12 Characterization and hydrogen storage performance of TiZrCrMnFeNi and TiZrNbFeNi alloy systems. XRD of the TiZrCrMnFeNi composition (a)[29] and its hydrogen storage performance as measured *via* PCT (b);[29] XRD of the TiZrNbFeNi (c)[34] and TiZrNbFeNi compositions (d)[34] and their hydrogen storage performance as measured *via* PCT for the first cycle (e)[34] and second cycle (f).[34] Reprinted (adapted or reprinted in part) with permission.[29] Copyright 2019, Acta Materialia Inc. Published by Elsevier Ltd. Reprinted (adapted or reprinted in part) with permission.[34] Copyright 2020, Hydrogen Energy Publications LLC. Published by Elsevier Ltd.

B elements in the alloy systems might help in the desorption of hydrogen from stable hydrides, and therefore increase the reversible storage capacity.[17,34]

The TiZrCrMnFeNi and TiZrNbFeNi alloy systems called attention due to their reported reversible hydrogen storage capacity at room temperature.[29,34] Edalati *et al.*[29] evaluated the hydrogen storage performance of TiZrCrMnFeNi *via* PCT isotherms and kinetic curves. They have reported that the alloy (with dominant C14 Laves phase Fig. 12a) absorbed 1.6 wt% H_2 at room temperature and without prior activation process in the first hydrogenation/dehydrogenation cycle. According to the authors, the VEC parameter might have played an important role in the reversibility shown at room temperature since it was used as a criterion in the design of the alloy composition. The VEC value of 6.4 was used because it was suggested by Nygard *et al.*[23] that this value would allow dehydrogenation at room temperature. Even though this suggestion was made based on the analysis of disordered solid solutions, Edalati *et al.*[29] applied it to intermetallic HEAs. The hydrogen storage behavior is maintained upon cycling, and complete hydrogen desorption is achieved. It should be noted that the absorbed amount increases up to 1.7 wt% H_2 in the third cycle, as shown in Fig. 12b. Moreover, no hysteresis in the PCT isotherms has been observed. The kinetics investigations showed that the material had reached the maximum capacity in less than one minute. The authors pointed out that the observed capacity for this alloy is close to the theoretical value estimated for AB_2H_3 hydride systems. Moreover, the capacity of the investigated alloy is comparable to those of traditional materials for room temperature hydrogen storage, such as $LaNi_5$ and TiFe. The advantages of this HEA are that no activation process is needed, and the alloy presents good resistance to the air atmosphere.

The same group investigated the hydrogen storage performance of the equiatomic TiZrNbFeNi and the non-equiatomic $Ti_{20}Zr_{20}Nb_5Fe_{40}Ni_{15}$ alloys (both with dominant C14 Laves phase Fig. 12c and d) *via* PCT isotherms obtained at room temperature without prior activation process. It was reported that both compositions absorbed and desorbed hydrogen at room temperature. The values of the VEC parameter also guided the design of these alloys. The equiatomic composition presented higher capacity in the first cycle than the non-equiatomic one. However, in the second cycle, the capacity of the non-equiatomic exceeded that of the equiatomic alloy since the equiatomic composition presented a significant capacity loss, while the capacity loss of the non-equiatomic alloy was slight (Fig. 12e and f). The reasons behind these reversibility performances can be related to the chemical composition and the volume of the unit cell. The presence of more hydride forming elements in the equiatomic composition and the higher unit cell volume observed for this alloy resulted in the higher capacity that this composition presented in the first cycle. It was proposed that the differences observed in the second cycle are related to the retention of hydrogen in the structure after desorption at room temperature. It means that the equiatomic alloy retained a considerable amount of hydrogen after desorption (in an expanded structure), causing substantial capacity loss upon cycling, while this retention was a minor issue in the non-equiatomic alloy. In this study, it was also pointed out that considering the limited number of materials with reversible hydrogen storage capacity at room

temperature, the reported results suggest the significance of this kind of HEA composition.[34]

Perspectives of intermetallic HEAs

The results of hydrogen storage performance reported so far for the investigated intermetallic HEAs are in general similar to those of traditional intermetallic compounds, such as $LaNi_5$ and TiFe.[2,29,34] In terms of H/M, no alloy system or composition was identified yet that presented an abnormal capacity of storing more hydrogen per metal atom than the structures of the traditional intermetallic compounds. Consequently, particularly in the case of intermetallic forming compositions based just on transition metals, the molar weight of these alloys may limit their potential due to limited gravimetric hydrogen storage capacity.

Nevertheless, very promising results have already been reported in terms of compositions that presented good reversible hydrogen storage capacity at room temperature without the need for an activation process.[29,34] As for BCC solid solution HEAs, it seems that VEC is also an important parameter for the analysis of the stability of the hydrides formed from intermetallic HEAs. Considering that there is a limited number of materials that present this kind of reversibility at room temperature, the reported results make these kinds of intermetallic HEAs promising solutions for stationary applications, which require low temperatures (for energy efficiency) but are not strict in terms of weight of the system.[29,34] Additionally, we suggest further investigations on the relation of the local and bulk structure of intermetallic HEAs and the hydrogen storage reversibility present by them.

Various intermetallic structures have been described in the literature, which, apart from Laves phases, showed the ability to reversibly store hydrogen, such as Haucke phases, hexagonal structures, and cubic structures.[121] In the case of Laves phases, C15 is also considered a promising structure for hydrogen storage. C15 and other intermetallic structures have already been synthesized using HEA compositions, although single-phase intermetallics are less frequently obtained than single-phase disordered solid solutions.[40] Therefore, it is opportune to point out that investigations of intermetallic HEAs for hydrogen storage with structures different from C14 Laves are missing in the literature.

Intermetallic forming compositions have also been investigated to synthesize metal hydrides with high equilibrium pressure (unstable hydrides).[8] These hydrides, combined with pressurized hydrogen, are considered a good solution for hydrogen storage *via* hybrid hydrogen storage tanks. In this regard, it is also worth pointing out that investigations of intermetallic HEAs capable of forming unstable hydrides are missing.

Conclusions

One of the main challenges for implementing hydrogen technologies is the hydrogen storage aspect. Metal hydrides have been investigated for decades, and they are considered a long-term alternative for many hydrogen storage applications. In this regard, a new class of alloys, namely high-entropy alloys, brought new and promising possibilities in the investigations of metal hydrides. Superior storage capacities have been reported for HEAs, but it needs further pieces of evidence. The main interesting and promising aspect of HEAs is their vastness of compositions, which in terms of hydrogen storage applications offers enormous opportunities since different structures can be formed (BCCs, Laves, and HCPs), and the hydrogenation properties can be significantly tuned, as the reports published so far indicate.

Given the current state of knowledge, the greatest necessity for the progress of the field is the development and testing of effective methods to navigate into the compositional vastness. It is essential since systematic studies (classical approach using alloying or elemental substitution) present limited capacity in this case (impractical considering the vast number of compositions). This review shows that screening and predictive methods are needed to correlate the alloy composition with phase formation and stability and finally with the hydrogen storage properties (thermodynamic properties). A great effort has been put on the first aspect by the broad HEA community with considerable progress by using methods such as CALPHAD (using a thermodynamic equilibrium approach), *ab initio* calculations (for a better assessment of specific compositions), and combinatorial methods (for investigations of a broad range of compositions and metastable phases). However, only a few attempts have been made to model the hydrogenation properties of HEAs. Here, we highlighted the importance of modeling the hydrogenation behavior of these alloys by exposing two recent attempts that are based on thermodynamics and data science. We think that the improvement and use of this kind of tool to assess the full potential of HEAs for hydrogen storage is highly significant. The modeling of the thermodynamic properties of HEA-H systems, together with the phase formation and stability assessment methods, may allow the development of powerful high throughput techniques, which will favor a better investigation of HEA compositions for hydrogen storage. The modeling may also provide the path for effective incorporation and consolidation of machine learning techniques into this research field, which could be considered the state of the art of many materials science and engineering fields.

Alloy design, synthesis, and processing methods are of great importance not just for research and development but also for technology implementation. Melting processes (especially arc melting) have been often used by the hydrogen storage community as it is a conventional process and relatively facilitates structure and microstructure characterization (due to the synthesis of structures with fewer defects). Milling processes (high energy ball milling) are useful for synthesizing compositions with low alloying affinity (positive mixing enthalpies) and a tendency to segregate.

Among the HEAs investigated so far, those that form BCC structures are promising for reversible hydrogen storage. This group of alloys can absorb high amounts of hydrogen, with H/M up to 2. Moreover, the hydrogen properties of these alloys

can be significantly modified based on the alloy composition. For example, some of the alloys absorb hydrogen at room temperature, while others need elevated temperatures to react with hydrogen. In this regard, two alloys can be highlighted ($Ti_{0.325}V_{0.275}Zr_{0.125}Nb_{0.275}$ and TiVCrNb) as they presented the capacity of absorbing hydrogen at room temperature, similarly to the V–H system, with the advantage (for some applications as stationary hydrogen storage, for example) that the equilibrium pressures for the dihydride formation are moderate compared to the V–H system. Concerning the BCC HEAs, it is suggested that further attention should be put on the investigations on their dehydrogenation processes (conditions for effectively desorbing hydrogen and occurrence of segregation, for example), the average and local role of VEC in the hydrogen storage behavior, and the influence of the synthesis and processing methods.

The lightweight HEAs investigated to date are composed of 10–57% of light elements (Mg, Al). Although the use of higher fractions of light elements is advantageous in decreasing the alloy molar weight, the low number of already reported studies in this field indicates challenges in developing this concept. One of them is mixing the elements for obtaining solid solutions since light elements, such as Mg, present non-favorable enthalpies of mixing with transition metals. The other seems to be related to the positive enthalpy of hydrogen solution that some light elements present, which may limit the formation of fully hydrogenated structures. Despite this, the $Mg_{0.10}Ti_{0.30}V_{0.25}Zr_{0.10}Nb_{0.2}$ HEA composition has already been reported with promising hydrogen storage performance as it absorbed 1.7 H/M (2.7 wt% H_2) at room temperature with fast kinetics. Given the limited number of publications, more investigations are necessary for assessing the potential of similar compositions for hydrogen storage.

Concerning intermetallic HEAs, the reports published so far indicate that some materials present similar behavior as conventional intermetallic compounds. However, it has been already shown that intermetallic HEAs can also reversibly absorb large amounts of hydrogen at room temperature without needing an activation process. Considering the studies evaluated here, we consider that there is a promising space for investigations of HEAs with C14 Laves structure, HEAs that form other intermetallic structures and HEAs that have the potential to form unstable metal hydrides.

Finally, we suggest further investigations on the comparative behavior of HEAs that form disordered solid solutions (such as BCC HEAs) and intermetallic HEAs in terms of hydrogen storage. It could be interesting, at least out of scientific curiosity, to analyze systematically and comparatively how the intrinsic structures and compositions of these kinds of HEAs influence on the hydrogen storage properties presented by them.

Author contributions

Felipe Marques: conceptualization, writing – original draft, writing – review & editing. Mateusz Balcerzak: writing – original draft, visualization, writing – review & editing. Frederik Winkelmann: writing – original draft, visualization, writing – review & editing. Guilherme Zepon: conceptualization, writing – original draft, writing – review & editing. Michael Felderhoff: conceptualization, writing – review & editing, and funding acquisition.

Conflicts of interest

There are no conflicts to declare.

Acknowledgements

Funded by the Deutsche Forschungsgemeinschaft (DFG, German Research Foundation) – 449160425. Frederik Winkelmann is grateful for the financial support from the IMPRS SurMat (International Max-Planck Research School for Interface Controlled Materials for Energy Conversion) in Düsseldorf, Germany. Guilherme Zepon is grateful for the financial support from the Serrapilheira Institute (grant number Serra-1709-17362). Open Access funding provided by the Max Planck Society.

References

1 P. Jena, *J. Phys. Chem. Lett.*, 2011, **2**, 206–211.
2 B. Sakintuna, F. Lamari-Darkrim and M. Hirscher, *Int. J. Hydrogen Energy*, 2007, **32**, 1121–1140.
3 P. Dantzer, *Hydrogen Met. III*, 1997, vol. 73, pp. 279–340.
4 M. Dornheim, *Thermodynamics – Interaction Studies – Solids, Liquids and Gases*, 2011.
5 V. A. Yartys, M. V. Lototskyy, E. Akiba, R. Albert, V. E. Antonov, J. R. Ares, M. Baricco, N. Bourgeois, C. E. Buckley, J. M. Bellosta von Colbe, J. C. Crivello, F. Cuevas, R. v. Denys, M. Dornheim, M. Felderhoff, D. M. Grant, B. C. Hauback, T. D. Humphries, I. Jacob, T. R. Jensen, P. E. de Jongh, J. M. Joubert, M. A. Kuzovnikov, M. Latroche, M. Paskevicius, L. Pasquini, L. Popilevsky, V. M. Skripnyuk, E. Rabkin, M. V. Sofianos, A. Stuart, G. Walker, H. Wang, C. J. Webb and M. Zhu, *Int. J. Hydrogen Energy*, 2019, **44**, 7809–7859.
6 S. Kumar, A. Jain, T. Ichikawa, Y. Kojima and G. K. Dey, *Renewable Sustainable Energy Rev.*, 2017, **72**, 791–800.
7 E. M. Dematteis, N. Berti, F. Cuevas, M. Latroche and M. Baricco, *Mater. Adv.*, 2021, **2**, 2524.
8 A. Lys, J. O. Fadonougbo, M. Faisal, J.-Y. Suh, Y.-S. Lee, J.-H. Shim, J. Park and Y. W. Cho, *Hydrogen*, 2020, **1**, 38–63.
9 N. A. A. Rusman and M. Dahari, *Int. J. Hydrogen Energy*, 2016, **41**, 12108–12126.
10 Y. F. Kao, S. K. Chen, J. H. Sheu, J. T. Lin, W. E. Lin, J. W. Yeh, S. J. Lin, T. H. Liou and C. W. Wang, *Int. J. Hydrogen Energy*, 2010, **35**, 9046–9059.
11 I. Kunce, M. Polanski and J. Bystrzycki, *Int. J. Hydrogen Energy*, 2013, **38**, 12180–12189.
12 I. Kunce, M. Polanski and J. Bystrzycki, *Int. J. Hydrogen Energy*, 2014, **39**, 9904–9910.

13 M. Sahlberg, D. Karlsson, C. Zlotea and U. Jansson, *Sci. Rep.*, 2016, **6**, 1–6.
14 I. Kunce, M. Polański and T. Czujko, *Int. J. Hydrogen Energy*, 2017, **42**, 27154–27164.
15 G. Zepon, D. R. Leiva, R. B. Strozi, A. Bedoch, S. J. A. Figueroa, T. T. Ishikawa and W. J. Botta, *Int. J. Hydrogen Energy*, 2018, **43**, 1702–1708.
16 D. Karlsson, G. Ek, J. Cedervall, C. Zlotea, K. T. Møller, T. C. Hansen, J. Bednarčík, M. Paskevicius, M. H. Sørby, T. R. Jensen, U. Jansson and M. Sahlberg, *Inorg. Chem.*, 2018, **57**, 2103–2110.
17 S. K. Chen, P. H. Lee, H. Lee and H. T. Su, *Mater. Chem. Phys.*, 2018, **210**, 336–347.
18 J. Hu, H. Shen, M. Jiang, H. Gong, H. Xiao, Z. Liu, G. Sun and X. Zu, *Nanomaterials*, 2019, **9**, 461.
19 C. Zlotea, M. A. Sow, G. Ek, J.-P. Couzinié, L. Perrière, I. Guillot, J. Bourgon, K. T. Møller, T. R. Jensen, E. Akiba and M. Sahlberg, *J. Alloys Compd.*, 2018, **775**, 667–674.
20 C. Zhang, Y. Wu, L. You, X. Cao, Z. Lu and X. Song, *J. Alloys Compd.*, 2019, 613–620.
21 M. M. Nygård, G. Ek, D. Karlsson, M. Sahlberg, M. H. Sørby and B. C. Hauback, *Int. J. Hydrogen Energy*, 2019, **44**, 29140–29149.
22 J. Montero, C. Zlotea, G. Ek, J. C. Crivello, L. Laversenne and M. Sahlberg, *Molecules*, 2019, **24**, 2799.
23 M. M. Nygård, G. Ek, D. Karlsson, M. H. Sørby, M. Sahlberg and B. C. Hauback, *Acta Mater.*, 2019, **175**, 121–129.
24 M. M. Nygård, W. A. Sławiński, G. Ek, M. H. Sørby, M. Sahlberg, D. A. Keen and B. C. Hauback, *Acta Mater.*, 2020, **199**, 504–513.
25 H. Shen, J. Hu, P. Li, G. Huang, J. Zhang, J. Zhang, Y. Mao, H. Xiao, X. Zhou, X. Zu, X. Long and S. Peng, *J. Mater. Sci. Technol.*, 2020, **55**, 116–125.
26 S. K. Dewangan, V. K. Sharma, P. Sahu and V. Kumar, *Int. J. Hydrogen Energy*, 2020, **45**, 16984–16991.
27 C. Zhang, A. Song, Y. Yuan, Y. Wu, P. Zhang, Z. Lu and X. Song, *Int. J. Hydrogen Energy*, 2020, **45**, 5367–5374.
28 F. Marques, H. C. Pinto, S. J. A. Figueroa, F. Winkelmann, M. Felderhoff, W. J. Botta and G. Zepon, *Int. J. Hydrogen Energy*, 2020, **45**, 19539–19552.
29 P. Edalati, R. Floriano, A. Mohammadi, Y. Li, G. Zepon, H. W. Li and K. Edalati, *Scr. Mater.*, 2020, **178**, 387–390.
30 R. B. Strozi, D. R. Leiva, J. Huot, W. J. Botta and G. Zepon, *Int. J. Hydrogen Energy*, 2020, **46**, 2351–2361.
31 J. Montero, G. Ek, L. Laversenne, V. Nassif, G. Zepon, M. Sahlberg and C. Zlotea, *J. Alloys Compd.*, 2020, **835**, 155376.
32 G. Ek, M. M. Nygård, A. F. Pavan, J. Montero, P. F. Henry, M. H. Sørby, M. Witman, V. Stavila, C. Zlotea, B. C. Hauback and M. Sahlberg, *Inorg. Chem.*, 2020, **60**(2), 1124–1132.
33 M. M. Nygård, Ø. S. Fjellvåg, M. H. Sørby, K. Sakaki, K. Ikeda, J. Armstrong, P. Vajeeston, W. A. Sławiński, H. Kim, A. Machida, Y. Nakamura and B. C. Hauback, *Acta Mater.*, 2020, 116496.
34 R. Floriano, G. Zepon, K. Edalati and A. Mohammadi, *Int. J. Hydrogen Energy*, 2020, **45**, 33759–33770.
35 J. Montero, G. Ek, M. Sahlberg and C. Zlotea, *Scr. Mater.*, 2021, **194**, 113699.
36 K. R. Cardoso, V. Roche, A. M. Jorge, F. J. Antiqueira, G. Zepon and Y. Champion, *J. Alloys Compd.*, 2021, **858**, 158357.
37 M. O. de Marco, Y. Li, H. W. Li, K. Edalati and R. Floriano, *Adv. Eng. Mater.*, 2020, **22**, 1901079.
38 B. Cantor, I. T. H. Chang, P. Knight and A. J. B. Vincent, *Mater. Sci. Eng., A*, 2004, **375–377**, 213–218.
39 J. W. Yeh, S. K. Chen, S. J. Lin, J. Y. Gan, T. S. Chin, T. T. Shun, C. H. Tsau and S. Y. Chang, *Adv. Eng. Mater.*, 2004, **6**, 299–303.
40 D. B. Miracle and O. N. Senkov, *Acta Mater.*, 2017, **122**, 448–511.
41 H. Yao, J.-W. Qiao, M. Gao, J. Hawk, S.-G. Ma and H. Zhou, *Entropy*, 2016, **18**, 189.
42 B. Gludovatz, A. Hohenwarter, K. V. S. Thurston, H. Bei, Z. Wu, E. P. George and R. O. Ritchie, *Nat. Commun.*, 2016, **7**, 1–8.
43 L. B. Wang, H. T. Yuan, Y. J. Wang, H. B. Yang, Q. D. Li, Y. N. Lin and Y. S. Zhang, *J. Alloys Compd.*, 2001, **319**, 242–246.
44 S. v. Mitrokhin, *J. Alloys Compd.*, 2005, **404–406**, 384–387.
45 Z. Cao, L. Ouyang, H. Wang, J. Liu, L. Sun and M. Zhu, *J. Alloys Compd.*, 2015, **639**, 452–457.
46 E. Akiba and H. Ibab, *Intermetallics*, 1998, **6**, 461470.
47 X. Yu, Z. Wu, B. Xia, T. Huang, J. Chen, Z. Wang and N. Xu, *J. Mater. Res.*, 2003, **18**, 2533–2536.
48 C. Zhou, H. Wang, L. Z. Ouyang, J. W. Liu and M. Zhu, *J. Alloys Compd.*, 2019, **806**, 1436–1444.
49 J. Huot, E. Akiba and H. Iba, *J. Alloys Compd.*, 1995, **228**, 181–187.
50 Y. Tsushio and E. Akiba, *J. Alloys Compd.*, 1998, **267**, 246–251.
51 E. P. George, D. Raabe and R. O. Ritchie, *Nat. Rev. Mater.*, 2019, **4**, 515–534.
52 K. T. Butler, D. W. Davies, H. Cartwright, O. Isayev and A. Walsh, *Nature*, 2018, **559**, 547–555.
53 Q. Lai, Y. Sun, T. Wang, P. Modi, C. Cazorla, U. B. Demirci, J. R. Ares Fernandez, F. Leardini and K. F. Aguey-Zinsou, *Adv. Sustainable Syst.*, 2019, **3**, 1–64.
54 M. Felderhoff, C. Weidenthaler, R. von Helmolt and U. Eberle, *Phys. Chem. Chem. Phys.*, 2007, **9**, 2643–2653.
55 C. Weidenthaler and M. Felderhoff, *Energy Environ. Sci.*, 2011, **4**, 2495–2502.
56 K. Uenishi, K. F. Kobayashi, K. N. Ishihara and P. H. Shingu, *Mater. Sci. Eng., A*, 1991, **134**, 1342–1345.
57 M. Witman, G. Ek, S. Ling, J. Chames, S. Agarwal, J. Wong, M. D. Allendorf, M. Sahlberg and V. Stavila, *Chem. Mater.*, 2021, **33**(11), 4067–4076.
58 G. Zepon, B. H. Silva, C. Zlotea, W. J. Botta and Y. Champion, *Acta Mater.*, 2021, **215**, 117070.
59 K. Momma and F. Izumi, *J. Appl. Crystallogr.*, 2011, **44**, 1272–1276.
60 W. Hume-Rothery and H. M. Powell, *Z. Kristallogr. - Cryst. Mater.*, 1935, **91**, 23–47.

61 S. Guo, C. Ng, J. Lu and C. T. Liu, *J. Appl. Phys.*, 2011, **109**, 103505.
62 X. Yang and Y. Zhang, *Mater. Chem. Phys.*, 2012, **132**, 233–238.
63 Y. Zhang, Y. J. Zhou, J. P. Lin, G. L. Chen and P. K. Liaw, *Adv. Eng. Mater.*, 2008, **10**, 534–538.
64 S. Guo, *Mater. Sci. Technol.*, 2015, **31**, 1223–1230.
65 A. Takeuchi and A. Inoue, *Mater. Trans.*, 2005, **46**, 2817–2829.
66 O. N. Senkov, J. D. Miller, D. B. Miracle and C. Woodward, *Calphad*, 2015, **50**, 32–48.
67 S. S. Mishra, T. P. Yadav, O. N. Srivastava, N. K. Mukhopadhyay and K. Biswas, *J. Alloys Compd.*, 2020, **832**, 153764.
68 N. Yurchenko, N. Stepanov and G. Salishchev, *Mater. Sci. Technol.*, 2017, **33**, 17–22.
69 M. C. Troparevsky, J. R. Morris, P. R. C. Kent, A. R. Lupini and G. M. Stocks, *Phys. Rev. X*, 2015, **5**, 11041.
70 M. C. Troparevsky, J. R. Morris, M. Daene, Y. Wang, A. R. Lupini and G. M. Stocks, *JOM*, 2015, **67**, 2350–2363.
71 D. J. M. King, S. C. Middleburgh, A. G. McGregor and M. B. Cortie, *Acta Mater.*, 2016, **104**, 172–179.
72 B. H. Silva, C. Zlotea, Y. Champion, W. J. Botta and G. Zepon, *J. Alloys Compd.*, 2021, **865**, 158767.
73 T. B. Flanagan and W. A. Oates, *J. Alloys Compd.*, 2005, **404–406**, 16–23.
74 T. B. Flanagan and W. A. Oates, in *Hydrogen in Intermetallic Compounds I, Topics in Applied Physics*, ed. L. Schlapbach, Springer, Berlin, Heidelberg, 1988, vol. 63, pp. 49–85.
75 C. Zlotea, M. A. Sow, G. Ek, J. P. Couzinié, L. Perrière, I. Guillot, J. Bourgon, K. T. Møller, T. R. Jensen, E. Akiba and M. Sahlberg, *J. Alloys Compd.*, 2019, **775**, 667–674.
76 P. C. P. Bouten and A. R. Miedema, *J. Less-Common Met.*, 1980, **71**, 147–160.
77 J. Garcés, *Appl. Phys. Lett.*, 2010, **96**, 161904.
78 S. Qian and D. O. Northwood, *Int. J. Hydrogen Energy*, 1990, **15**, 649–654.
79 T. B. Flanagan and J. D. Clewley, *J. Less-Common Met.*, 1982, **83**, 127–141.
80 A. Y. Esayed and D. O. Northwood, *Int. J. Hydrogen Energy*, 1992, **17**, 211–218.
81 T. B. Flanagan, H. S. Chung and P. Choong-Nyeon, *J. Less-Common Met.*, 1986, **125**, 247–260.
82 S. Qian and D. O. Northwood, *Int. J. Hydrogen Energy*, 1988, **13**, 25–35.
83 K. H. J. Buschow, P. C. P. Bouten and A. R. Miedema, *Rep. Prog. Phys.*, 1982, **45**, 937–1039.
84 N. Otani, A. Kuwabara, T. Ogawa, C. A. J. Fisher, I. Tanaka and E. Akiba, *Int. J. Hydrogen Energy*, 2019, **44**, 28909–28918.
85 M. Rkhis, A. Alaoui-Belghiti, S. Laasri, S. Touhtouh, A. Hajjaji, E. K. Hlil, L. Bessais, D. Soubane, K. Zaidat and S. Obbade, *Int. J. Hydrogen Energy*, 2019, **44**, 23188–23195.
86 N. Bourgeois, J. C. Crivello, P. Cenedese and J. M. Joubert, *ACS Comb. Sci.*, 2017, **19**, 513–523.
87 Y. Bouhadda, A. Rabehi, Y. Boudouma, N. Fenineche, S. Drablia and H. Meradji, *Int. J. Hydrogen Energy*, 2009, **34**, 4997–5002.
88 T. J. Frankcombe, *J. Alloys Compd.*, 2007, **446–447**, 455–458.
89 K. C. Kim, A. D. Kulkarni, J. K. Johnson and D. S. Sholl, *Phys. Chem. Chem. Phys.*, 2011, **13**, 7218–7229.
90 K. C. Kim, A. D. Kulkarni, J. K. Johnson and D. S. Sholl, *Phys. Chem. Chem. Phys.*, 2011, **13**, 21520–21529.
91 M. Witman, S. Ling, D. M. Grant, G. S. Walker, S. Agarwal, V. Stavila and M. D. Allendorf, *J. Phys. Chem. Lett.*, 2020, **11**, 40–47.
92 V. Zadorozhnyy, B. Sarac, E. Berdonosova, T. Karazehir, A. Lassnig, C. Gammer, M. Zadorozhnyy, S. Ketov, S. Klyamkin and J. Eckert, *Int. J. Hydrogen Energy*, 2020, **45**, 5347–5355.
93 B. Sarac, V. Zadorozhnyy, E. Berdonosova, Y. P. Ivanov, S. Klyamkin, S. Gumrukcu, A. S. Sarac, A. Korol, D. Semenov, M. Zadorozhnyy, A. Sharma, A. L. Greer and J. Eckert, *RSC Adv.*, 2020, **10**, 24613–24623.
94 G. Ou, D. Li, W. Pan, Q. Zhang, B. Xu, L. Gu, C. Nan and H. Wu, *Adv. Mater.*, 2015, **27**, 2589–2594.
95 G. Briickmann and H. Scholz, *Handbook of Vacuum Arc Science and Technology*, 1996.
96 Z. Li, A. Ludwig, A. Savan, H. Springer and D. Raabe, *J. Mater. Res.*, 2018, **33**, 3156–3169.
97 C. Suryanarayana, *Mechanical alloying and milling*, 2004.
98 W. Wolf, S. A. Kube, S. Sohn, Y. Xie, J. J. Cha, B. E. Scanley, C. S. Kiminami, C. Bolfarini, W. J. Botta and J. Schroers, *Sci. Rep.*, 2019, **9**, 1–11.
99 R. Mertens, Z. Sun, D. Music and J. M. Schneider, *Adv. Eng. Mater.*, 2004, **6**, 903–907.
100 S. Kumar, A. Jain, T. Ichikawa, Y. Kojima and G. K. Dey, *Renewable Sustainable Energy Rev.*, 2017, **72**, 791–800.
101 S. Yang, F. Yang, C. Wu, Y. Chen, Y. Mao and L. Luo, *J. Alloys Compd.*, 2016, **663**, 460–465.
102 M. Balcerzak, *Int. J. Hydrogen Energy*, 2017, **42**, 23698–23707.
103 C. Zhang, Y. Wu, L. You, W. Qiu, Y. Zhang, Y. Yuan, Z. Lu and X. Song, *Scr. Mater.*, 2020, **178**, 503–507.
104 S. Sleiman and J. Huot, *J. Alloys Compd.*, 2021, **861**, 158615.
105 H. Shen, J. Zhang, J. Hu, J. Zhang, Y. Mao, H. Xiao, X. Zhou and X. Zu, *Nanomaterials*, 2019, **9**, 248.
106 C. Kittel, *Introduction to solid state physics*, Wiley, New York, 8th edn, 2005.
107 T. Schober and H. Wenzl, *Hydrogen in Met 2*, Topics in Applied Physics, Springer-Verlag, 1978, vol. 29, pp. 11–71.
108 J. Hu, J. Zhang, H. Xiao, L. Xie, H. Shen, P. Li, J. Zhang, H. Gong and X. Zu, *Inorg. Chem.*, 2020, **59**, 9774–9782.
109 S. Kumar, A. Jain, T. Ichikawa, Y. Kojima and G. K. Dey, *Renewable Sustainable Energy Rev.*, 2017, **72**, 791–800.
110 Target Explanation Document: Onboard Hydrogen Storage for Light-Duty Fuel Cell Vehicles|Department of Energy, https://www.energy.gov/eere/fuelcells/downloads/target-explanation-document-onboard-hydrogen-storage-light-duty-fuel-cell, accessed May 7, 2021.
111 H. W. Langmi, J. Ren, B. North, M. Mathe and D. Bessarabov, *Electrochim. Acta*, 2014, **128**, 368–392.

112 M. Mohan, V. K. Sharma, E. A. Kumar and V. Gayathri, *Energy Storage*, 2019, **1**, e35.
113 R. Li, J. Gao and K. Fa, *Mater. Sci. Forum*, 2010, **650**, 265–271.
114 R. Li, J. C. Gao and K. Fan, *Mater. Sci. Forum*, 2011, **686**, 235–241.
115 K. M. Youssef, A. J. Zaddach, C. Niu, D. L. Irving and C. C. Koch, *Mater. Res. Lett.*, 2014, **3**, 95–99.
116 C. Suryanarayana, *Research*, 2019, **2019**, 1–17.
117 R. Griessen and T. Riesterer, *Hydrogen in Intermetallic Compounds I*, Springer Berlin Heidelberg, Berlin, Heidelberg, 1988.
118 E. M. Dematteis, A. Santoru, M. G. Poletti, C. Pistidda, T. Klassen, M. Dornheim and M. Baricco, *Int. J. Hydrogen Energy*, 2018, 1–11.
119 X. Zhang, Y. Liu, Z. Ren, X. Zhang, J. Hu, Z. Huang, Y. Lu, M. Gao and H. Pan, *Energy Environ. Sci.*, 2021, **14**, 2302–2313.
120 Y. Tan, Y. Zhu and L. Li, *Chem. Commun.*, 2015, **51**, 2368–2371.
121 A. Züttel, *Mater. Today*, 2003, 24–33.
122 J.-M. Joubert, M. Latroche, A. Percheron-Guégan and B. Schmitt, *Acta Mater.*, 2006, **54**, 713–719.
123 J. M. Joubert, M. Latroche, A. Percheron-Guégan and K. Yvon, *J. Alloys Compd.*, 2002, **330–332**, 208–214.
124 M. Bououdina, D. Grant and G. Walker, *Int. J. Hydrogen Energy*, 2006, **31**, 177–182.
125 J. J. Reilly and R. H. Wiswall, *Inorg. Chem.*, 1974, **13**, 218–222.
126 M. Bououdina, J. L. Soubeyroux, P. de Rango and D. Fruchart, *Int. J. Hydrogen Energy*, 2000, **25**, 1059–1068.
127 Z. Li, H. Wang, L. Ouyang, J. Liu and M. Zhu, *J. Alloys Compd.*, 2019, **787**, 158–164.
128 J. Puszkiel, J. M. Bellosta von Colbe, J. Jepsen, S. v. Mitrokhin, E. Movlaev, V. Verbetsky and T. Klassen, *Energies*, 2020, **13**, 2751.
129 Z. Cao, L. Ouyang, H. Wang, J. Liu, L. Sun, M. Felderhoff and M. Zhu, *Int. J. Hydrogen Energy*, 2016, **41**, 11242–11253.
130 M. Kandavel, V. v. Bhat, A. Rougier, L. Aymard, G. A. Nazri and J. M. Tarascon, *Int. J. Hydrogen Energy*, 2008, **33**, 3754–3761.